Next, we examined the requirement for Lats in the regulation of Yap localization during preimplantation development. The mouse has two *Lats* genes, both of which are expressed throughout preimplantation development (Figure 3A). Since null mutations in either gene do not disrupt preimplantation development (McPherson et al., 2004; St. John et al., 1999; Yabuta et al., 2007), we overexpressed a catalytically inactive (kinase dead; KD) variant of Lats2, designed to dominantly inhibit both Lats1 and Lats2. As predicted, embryos overexpressing *Lats2-KD* exhibited clearly reduced p-Yap levels (Figure 6D), as well as Yap accumulation in nuclei of inside cells (Figure 6E) and a significant increase in Cdx2 in inside cells (type III embryos) (Figures 6B and 6C). Finally, to genetically explore the role of Lats1/2, we generated a null allele of *Lats1*, and we examined embryos obtained from intercrossing *Lats1*$^{+/-}$; *Lats2*$^{+/-}$ mice. Consistent with the analysis of *Lats2-KD* overexpression, *Lats1*$^{-/-}$; *Lats2*$^{-/-}$ double mutant embryos exhibited nuclear accumulation of Yap and strong Cdx2 expression in inside cells (n = 6/7) (Figure 6F; Figure S2). Taken together, these observations strongly suggest that Lats1/2 regulate Yap localization during preimplantation development.

Cell-Cell Contact Inhibits Nuclear Accumulation of Yap in Inside Cells

In cultured cells, the subcellular localization of Yap and therefore Tead activity are controlled by cell-cell contacts via the Hippo signaling pathway (Ota and Sasaki, 2008; Zhao et al., 2007). We therefore asked whether cell contact is also involved in the regulation of Yap localization in preimplantation embryos. To examine whether the degree of cell-cell contact can regulate the subcellular localization of Yap in three-dimensional cell aggregates, we first examined its localization in cultured aggregates of a mouse ES cell line, EB5. Yap was detected only in the cytoplasm of cells internal to the aggregates, whereas Yap was detected in the nucleus and cytoplasm of outer cells of aggregates (Figure 6G, left). Similar results were obtained for aggregates of an epithelial cell line, MTD1A (Figure 6G, right). These correlative results suggest that circumferential cell contacts may inhibit the nuclear localization of Yap.

We next disrupted E-cadherin-mediated cell adhesion by using the E-cadherin blocking antibody ECCD1. As reported (Shirayoshi et al., 1983), treatment of compacted 8-cell embryos with ECCD1 led to decompaction. Culture of these embryos led to the reestablishment of cell adhesion, recompaction, and blastocoel formation, although the timing of this latter process was premature, resulting in ICM sizes that were either small or undetectable (Figure 6H; Figure S3; data not shown) (Shirayoshi et al., 1983). As expected based on the severe reduction of ICM in older ECCD1-treated embryos, Yap was not strictly excluded from nuclei of inside cells among ECCD1-treated embryos examined shortly after recompacting (18- to 22-cell stages, n = 6/8) (Figure 6I, middle). In fact, inside cells exhibited levels of nuclear Yap comparable to those of outside cells in some embryos (n = 2/8) (Figure 6I, right). Conversely, p-Yap levels were clearly reduced in inside cells of ECCD1-treated embryos (Figure 6J). Thus, continuous maintenance of circumferential cell-cell contact or adhesion is a prerequisite for the proper regulation of Yap phosphorylation and repression of Yap accumulation in the nuclei of inside cells.

Cell Position Can Regulate Yap Localization and Cell Fate

The observation that the degree of cell contact correlates with Yap localization and activity provided a potential link between embryo topology and cell fate specification. To test this hypothesis, we examined Yap localization and Cdx2 expression after the manipulation of cell position, by using two different approaches. First, we forced cells to occupy an inside position in reaggregated embryos. Embryos were dissociated at the 8-cell stage, a stage at which Yap is nuclear in all cells, and prior to the creation of inside cells. In nondissociated 8-cell embryos, apicobasal cell polarization can be visualized by examining Ezrin, which localizes to the apical cell pole (Louvet-Vallee et al., 2001). However, in individual 1/8 blastomeres, this pattern was lost, as was nuclear Yap (Figure 7A). Next, we aggregated individual blastomeres from three different embryos into one large chimera, with some cells now occupying a position internal to the others. In these reaggregated embryos, outside cells reestablished polarity, and nuclear Yap and Cdx2 were detected. In contrast, neither nuclear Yap nor Cdx2 were detected in inside cells (Figure 7B).

As a second approach to manipulating cell position, we examined the dynamics of Yap localization and Cdx2 expression in the regenerating TE after immunosurgery (Rossant and Lis, 1979; Spindle, 1978). After immunosurgery, most embryos had reestablished a morphologically distinct TE layer and blastocoel by 24 hr (n = 4/7), and nuclear Yap and Cdx2 were detected in outside cells of all regenerates (Figure 7C, n = 7/7). At 12 hr after immunosurgery, some cells appeared to be flattening on the surface of the ICM (n = 5/5), and nuclear Yap and Cdx2 were detected in these cells, although levels were apparently weaker compared with levels seen in later stages of regeneration (Figure 7D, n = 4/5). Together, these observations support the hypothesis that cell position influences the cell fate in preimplantation embryos by regulating subcellular localization of Yap.

DISCUSSION

Tead4 Instructively Regulates Multiple Transcription Factors to Promote Trophoblast Development

Although *Tead4* is required for *Cdx2* expression in vivo, the unpatterned expression of *Tead4* (Nishioka et al., 2008) made it difficult to predict that Tead4 restricts Cdx2 expression to outside cells during TE formation. We have shown that the activity of Tead4 is regulated, and that its activation is sufficient to regulate multiple factors in parallel to promote trophoblast fate specification in the ES cell model (Figure 7E). These observations are consistent with our analysis of *Tead4* mutant embryos (Nishioka et al., 2008), and with the fact that the *Tead4* mutant phenotype is more severe than loss of *Cdx2* alone (Strumpf et al., 2005). Thus, Tead4 appears to act at the top of a hierarchy of trophoblast-specific transcription factors, among which *Cdx2* plays a central role. However, we do not yet know whether Tead4 regulates *Cdx2* directly, since the *Cdx2* trophoblast enhancer has not been identified. Whereas Tead4-Yap activates Cdx2 in the outer cells, the uniform expression of Oct3/4 up to the late blastocyst stage would suggest that *Cdx2* receives persistent suppressive input from Oct3/4 (Dietrich and Hiiragi, 2007; Niwa et al., 2005). Tead4 may, therefore, promote Cdx2

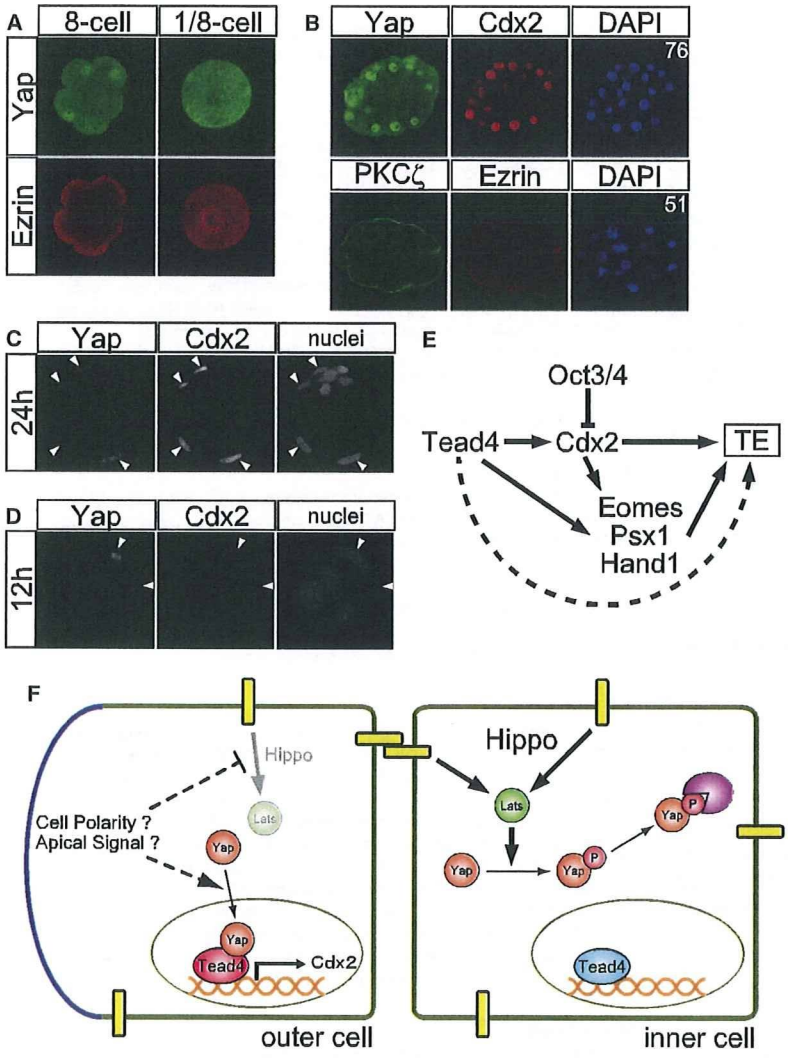

Figure 7. Cell Position Controls Nuclear Localization of Yap

(A) Altered Yap localization and cell polarity (Ezrin) in dissociated blastomeres of the 8-cell embryo.

(B) Localization of Yap, PKCζ, and Ezrin in reaggregated embryos.

(C and D) Yap localization and Cdx2 expression in isolated inner cell masses (C) 24 hr and (D) 12 hr after immunosurgery. Arrowheads indicate Yap-positive nuclei.

(E) A model of the transcriptional network regulating TE development.

(F) A model of cell position-dependent fate specification in preimplantation embryos. See Discussion for details.

expression by overcoming this negative input. Thus, Tead4 instructively regulates multiple transcription factors to promote trophoblast development.

Lats and Yap Convert Positional Information into Cell Fate Information

Two classical models of cell fate specification during preimplantation development are the Inside-Outside Model, in which, topological differences dictate cell fates (Tarkowski and Wroblewska, 1967), and the Polarity Model, wherein differential inheritance of information present along the apicobasal axis dictates both cell position and fate (Johnson and Ziomek, 1981). These models are not mutually exclusive and provide a framework for interpreting our results (Figure 7F). As we have shown, two components of the Hippo signaling pathway, Lats and Yap, are involved in the establishment of position-dependent Tead4 activity and cell fate specification. In inside cells, Yap is phosphorylated by Lats and is excluded from the nuclei. As a consequence, Tead4 remains inactive, and these cells adopt an ICM fate. In the outside cells, lower levels of Yap phosphorylation allow for its nuclear accumulation, which leads to activation of Tead4. In turn, active Tead4 induces trophoblast genes, including *Cdx2*, and promote TE fate.

Although cell position appears to influence Yap localization, the exact mechanisms underlying this phenomenon remain elusive. One likely mechanism is the difference in the degree of cell-cell contacts. Inside cells are surrounded entirely by outside cells, whereas outside cells have an outside-exposed surface. Thus, the degree of cell contact could influence Lats- and/or Hippo-mediated cell signaling. Cell contact-based changes in Hippo signaling have been proposed to explain cell contact-mediated inhibition of proliferation in cultured cells (Ota and Sasaki, 2008; Zhao et al., 2007), and cell contacts are actually required for the suppression of nuclear Yap in inside cells of preimplantation embryos.

Although our observations generally support the Inside-Outside model of early lineage specification, they do not rule out involvement of the Polarity Model. In addition to cell-cell contact, other information, such as cell polarization or the presence of an exposed apical surface, may also contribute to differential Yap localization in the early embryo, for example by restricting the localization or activity of Hippo signaling components. In support of this, dissociated blastomeres, which do not receive cell contact information and also lose polarity, did not exhibit nuclear Yap. As two transmembrane receptors, Fat and CD44, are known upstream regulators of Hippo signaling (Bennett and Harvey, 2006; Hamaratoglu et al., 2006; Morrison et al., 2001; Silva et al., 2006; Willecke et al., 2006), it is tempting to speculate that signaling through these proteins may transmit cell contact information to Lats/Yap in preimplantation embryos.

Although recently it has been shown that Ras-MAPK signaling promotes TE development (Lu et al., 2008), its relationship to Tead4-Yap remains unknown. Interestingly, MAPK signaling negatively regulates Tead activity in cultured cells (Thompson et al., 2003).

Our model places importance on the suppression of Tead4 activity in inside cells to establish differential Tead4 activity along the inside-outside axis. Active Tead4 induces and/or reinforces *Cdx2* expression, overcoming Oct3/4-mediated repression in outside cells, whereas inactive Tead4 together with Oct3/4 may suppress *Cdx2* expression in inside cells. Inactive Tead4 likely acts as a repressor and suppresses *Cdx2* expression, as switching roles between activator and repressor is a typical feature of transcription factors at the end of signaling pathways (Barolo and Posakony, 2002). Continuous operation of this mechanism throughout preimplantation development likely ensures position-dependent cell fate specification, whereas inside and outside daughters are produced from mothers that are initially outside (Fleming, 1987). This system would confer a degree of developmental flexibility on preimplantation mouse embryos. Recently identified asymmetric distribution of *Cdx2* mRNA (Jedrusik et al., 2008) may also be involved in this process.

A Role for Hippo Signaling in Preimplantation Embryos

The Hippo signaling pathway mediates cell contact-mediated growth inhibition in cultured cells (Lei et al., 2008; Ota and Sasaki, 2008; Zhao et al., 2007, 2008), but our evidence suggests a slightly different role during preimplantation development. Although cell contact is still involved, growth inhibition is not, since changes in Yap localization suppressed Cdx2 expression without affecting cell number. A similar role in cell fate specification has been observed in *Drosophila* photoreceptor differentiation (Mikeladze-Dvali et al., 2005), suggesting that Hippo signaling may regulate distinct cellular outcomes, depending on the context.

EXPERIMENTAL PROCEDURES

Cell Culture

EB5 ES cells were cultured on gelatin-coated dishes in the absence of feeder cells in ES medium (Glasgow modification of Eagle's medium (GMEM) supplemented with 10% (v/v) FCS, 1000 U/ml LIF, 1× sodium pyruvate, 1× nonessential amino acids, 10^{-4} M β-mercaptoethanol) (Niwa et al., 1998) containing 10 μg/ml blasticidin S. 5ECER4 ES cells (Niwa et al., 2005) were cultured in ES medium containing 10 μg/ml blasticidin S and 1 μg/ml puromycin. To establish ES cells stably expressing Tead4VP16ER (5TVER7 and 5TVER16), EB5 ES cells were electroporated with linearized pCAG-Tead4VP16ER-IP and were selected with 1 μg/ml puromycin in ES cell medium containing 10 μg/ml blasticidin S. *Tead4*$^{-/-}$ ES cells and derivatives were maintained in serum-free CultiCell medium (Stem Cell Sciences, Japan) (Ogawa et al., 2004). To establish *Tead4*$^{-/-}$ ES cells stably expressing Cdx2ER (T4CER9 and T4CER10), *Tead4*$^{-/-}$ ES cells (#1–5) (Nishioka et al., 2008) were electroporated with linearized pCAG-Cdx2ER-IP (Niwa et al., 2005) and were selected with 1 μg/ml puromycin in CultiCell serum-free ES medium. To establish *Cdx2*$^{-/-}$ ES cells stably expressing Tead4VP16ER (CTVER5 and CTVER20), dko23-5 ES cells (Niwa et al., 2005) were electroporated with linearized pCAG-Tead4VP16ER-IP and selected with 1 μg/ml puromycin in ES cell medium containing 10 μg/ml blasticidin S and 200 μg/ml G418. In dko23-5 ES cells, expression of *Oct3/4* does not change during differentiation, because *Oct3/4* is expressed from a transgene (Niwa et al., 2005). To induce transgenes, 5ECER4, T4CER9, and T4CER10 were induced with 1 μg/ml tamoxifen in ES medium. 5TVER7 and 5TVER16 were induced with 0.1 μg/ml tamoxifen, and CTVER5 and CTVER20 were induced with 0.2 μg/ml tamoxifen; higher doses of tamoxifen resulted in significant cell death of 5TVER7, 5TVER16, CTVER5, and CTVER20. Induction of ES cell differentiation into TS cells was performed as previously described (Niwa et al., 2005).

ES cell transfection with siRNA was performed by using Lipofectamine 2000 as previously described (Hough et al., 2006), by using feeder-free conditions. For Oct3/4 knockdown, three predesigned Stealth siRNAs (Stealth Select RNAi) targeting *Oct3/4* (Pou5f1-MSS237605, Pou5f1-MSS237606, and Pou5f1-MSS237607) were obtained from Invitrogen. Pou5f1-MSS237605 and Pou5f1-MSS237606 clearly reduced *Oct3/4*, whereas Pou5f1-MSS237607 exhibited a weaker effect. The two former siRNAs were therefore used and produced similar results. The representative result with Pou5f1-MSS237605 siRNA is shown in a figure. The Stealth RNAi Negative Control Medium GC Duplex (Invitrogen) was used for control experiments.

MTD1A (Hirano et al., 1987), NIH 3T3, and HeLa cells were cultured in Dulbecco's Modified Eagle's Medium containing 10% Fetal Calf Serum (DMEM + 10% FCS).

For detailed information about plasmids, see Supplemental Data.

Luciferase Assay

NIH 3T3 or HeLa cells were seeded at a density of 1×10^5 cells/well on 12-well plates 24 hr before transfection. A DNA mixture consisting of effector (50 ng), pCMV-Gal4 (BD) or pCMV-Gal4-Tead4C (50 ng), pG4-TK-Luc (200 ng), and pCS2-β-gal (50 ng) were transfected for 24 hr with 2 μl FuGENE HD (Roche). Lysate preparation, luciferase, and β-galactosidase assays were performed as described (Sasaki et al., 1999). Luciferase activities were normalized to β-galactosidase activities. For each experiment, values from two samples were averaged and are presented with standard errors.

RT-PCR

Total RNA was isolated from ES cells or embryos by using Trizol reagent (Invitrogen) by following the manufacturer's instruction. cDNA was prepared from 1 μg total RNA by using Ready-To-Go You-Prime First-Strand Beads (GE Healthcare) or Superscript III reverse transcriptase (Invitrogen) and Oligo-dT primers (Invitrogen) per manufacturers' instructions. cDNA was diluted 1:200 for quantitative PCR reactions. Primers and conditions for Quantitative-PCR (Q-PCR) reactions for *Cdx2*, *Eomes*, *Psx1*, *Hand1*, *Itga7*, *Oct3/4*, *Sox2*, *Fgf4*, and *Gapdh* are described by Niwa et al. (2005). Q-PCR was performed by using SYBR Premix Ex Taq (Takara Bio, Kyoto Japan) and an ABI PRISM 7900HT (Applied Biosystems). Expression of each gene was normalized to the expression of *Gapdh*. Average results and standard errors from three independent measurements are presented.

Mouse Lines

Wild-type litters were obtained by crossing C57BL/6 and [C57BL/6xDBA]F1 mice. *Yap*^{tm1Smil} mice (Morin-Kensicki et al., 2006) were crossed with *Actb:Cre* transgenic mice to remove the neomycin cassette flanked by *loxP* sites. Resulting mice (*Yap*$^{-tm1}$) are referred to as *Yap* mutant mice in this paper. *Wwtr1* mutant mice (*Taz*^{lacZ}) were previously described (Makita et al., 2008). *Lats2* mutant mice were previously described (Yabuta et al., 2007). The *Lats1* mutant allele was generated by homologous recombination in ES cells in H.N.'s laboratory. Exon 1 (E1), containing a translation initiation codon, was replaced with a cassette containing the *Pgk* promoter, the *neomycin resistance* gene, and the *Pgk* polyA signal (Figure S4A), resulting in generation of a null allele. Details for the generation and characterization of *Lats1* mutants will be described elsewhere by N.Y. and H.N. Mice were housed in environmentally controlled rooms in the Laboratory Animal Housing Facility of the RIKEN Center for Developmental Biology, under the institutional guidelines for animal and recombinant DNA experiments.

Embryo Culture and Embryo Manipulation

Embryo culture was performed as previously described (Nishioka et al., 2008). Treatment of embryos with ECCD1 (Takara Bio, Kyoto Japan) was performed as previously described (Shirayoshi et al., 1983). Dissociation of 8-cell-stage embryos was performed as previously described (Dietrich and Hiiragi, 2007), and blastomeres were reaggregated by gentle rocking in U-bottom, MPC-coated 96-well plates (Nunc).

RNA Injection

Poly(A)-tailed RNA was synthesized from cDNAs cloned into the pcDNA3.1-poly(A)83 plasmid (Yamagata et al., 2005), and purified RNAs were injected into both blastomeres of 2-cell-stage embryos according to standard protocols (Hogan et al., 1994). Details of plasmids used are provided in Supplemental Data.

Immunofluorescent Staining

Immunofluorescent staining of embryos was performed by following standard protocols. Inside cells were identified by acquiring Z-series confocal images of the stained embryos with LSM510 META (Zeiss). Embryos were fixed in 4% paraformaldehyde in phosphate-buffered saline (PBS) for 15 min at room temperature, and then washed in PBS + 0.2% goat serum (PBSS) for 5 min. Embryos were subsequently permeabilized with 0.2% Triton X-100 in PBS for 20 min at room temperature, washed in PBSS for 5 min, blocked with 2% goat serum in PBS (blocking solution), and incubated overnight with primary antibodies diluted in blocking solution at 4°C. After washing in PBSS for 5 min, embryos were incubated with the following secondary antibodies diluted in PBSS for 1 hr at room temperature: Alexa Fluor 488 goat anti-rabbit (Molecular Probes, A11034; 1:4000) and/or Alexa Fluor 594 goat anti-mouse (Molecular Probes, A11005; 1:4000). Nuclei were visualized by staining with 4,6-diamidino-2-phenylindole dilactate (DAPI; Molecular Probes, D3571). For detection of p-Yap, all solutions up to primary antibody were supplemented with Phosphatase Inhibitor Cocktail (Nacalai Tesque, Kyoto, Japan) at 1:100. For λPPase treatment, ~10 embryos were incubated with 2000 U Lambda Protein Phosphatase (Sigma P9614) in 100 ml λPPase buffer supplied by the manufacturer at 30°C for 1 hr prior to blocking.

Statistics

Statistical analyses were performed with Prism4 statistical software (GraphPad) by using Fisher's exact probability test. For all comparisons, experimental results were compared with control results (*β-globin*-injected). For experiments shown in Figures 2, 4, and 6, the frequencies of type III embryos were compared. For experiments shown in Figure 5, frequencies of type IV embryos were compared. Statistically significant differences ($p < 0.05$) are indicated by asterisks.

Quantification of Immunofluorescent Signals

Confocal images of the stained embryos were acquired with LSM510 META (Zeiss). Average pixel intensities of the Yap and DAPI in nuclear cross-section were measured by using MetaMorph software (Molecular Devices). Yap nuclear signal values were normalized to the DAPI signal. Average values from multiple embryos are presented with standard deviation.

Immunosurgery

Embryos were harvested around E3.0, zonae pellucida were removed, and embryos were subsequently incubated with nonpreadsorbed rabbit anti-mouse lymphocyte antibody (Cedarlane) diluted 1:8 in KSOM for 25 min in a 37°C incubator. Embryos were washed through five droplets of KSOM and then incubated as described above in anti-rabbit Alexa Fluor 488 (1:400, Molecular Probes) for 15 min. Embryos were again washed in KSOM, and then incubated as described above for 8 min in guinea pig complement (Cedarlane) diluted 1:4 in KSOM, and lysed cells were removed by extensive flushing through a pulled glass needle. Resulting inner cell masses were screened for efficient removal of TE by brief examination of fluorescence signal by fluorescence microscopy. Efficiently lysed ICMs were then incubated in KSOM as described above until the indicated time points, then harvested for immunostaining and confocal analysis as described (Ralston and Rossant, 2008). Antibodies used included rabbit anti-YAP (Cell Signaling; 1:100); mouse anti-Cdx2 (Biogenex; 1:200); anti-mouse Alexa 546, anti-mouse Alexa 488, and Draq5 (Molecular Probes; all at 1:400), and all images were collected during a single confocal session with identical confocal settings.

SUPPLEMENTAL DATA

Supplemental Data include four figures, one table, Supplemental Experimental Procedures, and Supplemental References and can be found with this article online at http://www.cell.com/developmental-cell/supplemental/S1534-5807(09)00077-X.

ACKNOWLEDGMENTS

We thank H. Sato, M. Shibata, and M. Harano for their excellent technical assistance, K. Yamagata for a plasmid, and A. Ogura and K. Mekada for collecting *Lats1/2* mutant embryos. We are also grateful to the Laboratory for Animal Resources and Genetic Engineering for collecting mouse embryos and the housing of the mice. This work was supported by grants from RIKEN (H.S.), by grants-in-aid for Scientific Research (S and B) and for Encouragement of Young Scientists from Ministry of Education, Culture, Sports, Science, and Technology of Japan (N.Y. and H.N.), and by grant #13426 from the Canadian Institutes of Health Research (J.R.).

Received: August 22, 2008
Revised: November 28, 2008
Accepted: February 6, 2009
Published: March 16, 2009

REFERENCES

Barolo, S., and Posakony, J.W. (2002). Three habits of highly effective signaling pathways: principles of transcriptional control by developmental cell signaling. Genes Dev. *16*, 1167–1181.

Basu, S., Totty, N.F., Irwin, M.S., Sudol, M., and Downward, J. (2003). Akt phosphorylates the Yes-associated protein, YAP, to induce interaction with 14-3-3 and attenuation of p73-mediated apoptosis. Mol. Cell *11*, 11–23.

Bennett, F.C., and Harvey, K.F. (2006). Fat cadherin modulates organ size in *Drosophila* via the Salvador/Warts/Hippo signaling pathway. Curr. Biol. *16*, 2101–2110.

Dietrich, J.E., and Hiiragi, T. (2007). Stochastic patterning in the mouse preimplantation embryo. Development *134*, 4219–4231.

Dong, J., Feldmann, G., Huang, J., Wu, S., Zhang, N., Comerford, S.A., Gayyed, M.F., Anders, R.A., Maitra, A., and Pan, D. (2007). Elucidation of a universal size-control mechanism in *Drosophila* and mammals. Cell *130*, 1120–1133.

Fleming, T.P. (1987). A quantitative analysis of cell allocation to trophectoderm and inner cell mass in the mouse blastocyst. Dev. Biol. *119*, 520–531.

Goulev, Y., Fauny, J.D., Gonzalez-Marti, B., Flagiello, D., Silber, J., and Zider, A. (2008). SCALLOPED interacts with YORKIE, the nuclear effector of the hippo tumor-suppressor pathway in *Drosophila*. Curr. Biol. *18*, 435–441.

Hamaratoglu, F., Willecke, M., Kango-Singh, M., Nolo, R., Hyun, E., Tao, C., Jafar-Nejad, H., and Halder, G. (2006). The tumour-suppressor genes NF2/Merlin and Expanded act through Hippo signalling to regulate cell proliferation and apoptosis. Nat. Cell Biol. *8*, 27–36.

Hao, Y., Chun, A., Cheung, K., Rashidi, B., and Yang, X. (2008). Tumor suppressor LATS1 is a negative regulator of oncogene YAP. J. Biol. Chem. *283*, 5496–5509.

Hirano, S., Nose, A., Hatta, K., Kawakami, A., and Takeichi, M. (1987). Calcium-dependent cell-cell adhesion molecules (cadherins): subclass specificities and possible involvement of actin bundles. J. Cell Biol. *105*, 2501–2510.

Hogan, B., Beddington, R., Constantini, F., and Lacy, E. (1994). Manipulating the Mouse Embryo: Laboratory Manual, Second Edition (Cold Spring Harbor, NY: Cold Spring Harbor Laboratory Press).

Hossain, Z., Ali, S.M., Ko, H.L., Xu, J., Ng, C.P., Guo, K., Qi, Z., Ponniah, S., Hong, W., and Hunziker, W. (2007). Glomerulocystic kidney disease in mice with a targeted inactivation of Wwtr1. Proc. Natl. Acad. Sci. USA *104*, 1631–1636.

Hough, S.R., Clements, I., Welch, P.J., and Wiederholt, K.A. (2006). Differentiation of mouse embryonic stem cells after RNA interference-mediated silencing of OCT4 and Nanog. Stem Cells *24*, 1467–1475.

Huang, J., Wu, S., Barrera, J., Matthews, K., and Pan, D. (2005). The Hippo signaling pathway coordinately regulates cell proliferation and apoptosis by inactivating Yorkie, the *Drosophila* homolog of YAP. Cell *122*, 421–434.

Jedrusik, A., Parfitt, D.E., Guo, G., Skamagki, M., Grabarek, J.B., Johnson, M.H., Robson, P., and Zernicka-Goetz, M. (2008). Role of Cdx2 and cell polarity in cell allocation and specification of trophectoderm and inner cell mass in the mouse embryo. Genes Dev. *22*, 2692–2706.

Johnson, M.H., and Ziomek, C.A. (1981). The foundation of two distinct cell lineages within the mouse morula. Cell *24*, 71–80.

Lei, Q.Y., Zhang, H., Zhao, B., Zha, Z.Y., Bai, F., Pei, X.H., Zhao, S., Xiong, Y., and Guan, K.L. (2008). TAZ promotes cell proliferation and epithelial-mesenchymal transition and is inhibited by the hippo pathway. Mol. Cell. Biol. *28*, 2426–2436.

Louvet-Vallee, S., Dard, N., Santa-Maria, A., Aghion, J., and Maro, B. (2001). A major posttranslational modification of ezrin takes place during epithelial differentiation in the early mouse embryo. Dev. Biol. *231*, 190–200.

Lu, C.W., Yabuuchi, A., Chen, L., Viswanathan, S., Kim, K., and Daley, G.Q. (2008). Ras-MAPK signaling promotes trophectoderm formation from embryonic stem cells and mouse embryos. Nat. Genet. *40*, 921–926.

Mahoney, W.M., Jr., Hong, J.H., Yaffe, M.B., and Farrance, I.K. (2005). The transcriptional co-activator TAZ interacts differentially with transcriptional enhancer factor-1 (TEF-1) family members. Biochem. J. *388*, 217–225.

Makita, R., Uchijima, Y., Nishiyama, K., Amano, T., Chen, Q., Takeuchi, T., Mitani, A., Nagase, T., Yatomi, Y., Aburatani, H., et al. (2008). Multiple renal cysts, urinary concentration defects, and pulmonary emphysematous changes in mice lacking TAZ. Am. J. Physiol. *294*, F542–F553.

McPherson, J.P., Tamblyn, L., Elia, A., Migon, E., Shehabeldin, A., Matysiak-Zablocki, E., Lemmers, B., Salmena, L., Hakem, A., Fish, J., et al. (2004). Lats2/Kpm is required for embryonic development, proliferation control and genomic integrity. EMBO J. *23*, 3677–3688.

Mikeladze-Dvali, T., Wernet, M.F., Pistillo, D., Mazzoni, E.O., Teleman, A.A., Chen, Y.W., Cohen, S., and Desplan, C. (2005). The growth regulators warts/lats and melted interact in a bistable loop to specify opposite fates in *Drosophila* R8 photoreceptors. Cell *122*, 775–787.

Morin-Kensicki, E.M., Boone, B.N., Howell, M., Stonebraker, J.R., Teed, J., Alb, J.G., Magnuson, T.R., O'Neal, W., and Milgram, S.L. (2006). Defects in yolk sac vasculogenesis, chorioallantoic fusion, and embryonic axis elongation in mice with targeted disruption of Yap65. Mol. Cell. Biol. *26*, 77–87.

Morrison, H., Sherman, L.S., Legg, J., Banine, F., Isacke, C., Haipek, C.A., Gutmann, D.H., Ponta, H., and Herrlich, P. (2001). The NF2 tumor suppressor gene product, merlin, mediates contact inhibition of growth through interactions with CD44. Genes Dev. *15*, 968–980.

Nishioka, N., Nagano, S., Nakayama, R., Kiyonari, H., Ijiri, T., Taniguchi, K., Shawlot, W., Hayashizaki, Y., Westphal, H., Behringer, R.R., et al. (2005). Ssdp1 regulates head morphogenesis of mouse embryos by activating the Lim1-Ldb1 complex. Development *132*, 2535–2546.

Nishioka, N., Yamamoto, S., Kiyonari, H., Sato, H., Sawada, A., Ota, M., Nakao, K., and Sasaki, H. (2008). Tead4 is required for specification of trophectoderm in pre-implantation mouse embryos. Mech. Dev. *125*, 270–283.

Niwa, H., Burdon, T., Chambers, I., and Smith, A. (1998). Self-renewal of pluripotent embryonic stem cells is mediated via activation of STAT3. Genes Dev. *12*, 2048–2060.

Niwa, H., Miyazaki, J., and Smith, A.G. (2000). Quantitative expression of Oct-3/4 defines differentiation, dedifferentiation or self-renewal of ES cells. Nat. Genet. *24*, 372–376.

Niwa, H., Toyooka, Y., Shimosato, D., Strumpf, D., Takahashi, K., Yagi, R., and Rossant, J. (2005). Interaction between Oct3/4 and Cdx2 determines trophectoderm differentiation. Cell *123*, 917–929.

Ogawa, K., Matsui, H., Ohtsuka, S., and Niwa, H. (2004). A novel mechanism for regulating clonal propagation of mouse ES cells. Genes Cells *9*, 471–477.

Ota, M., and Sasaki, H. (2008). Mammalian Tead proteins regulate cell proliferation and contact inhibition as a transcriptional mediator of Hippo signaling. Development *135*, 4059–4069.

Palmieri, S.L., Peter, W., Hess, H., and Scholer, H.R. (1994). Oct-4 transcription factor is differentially expressed in the mouse embryo during establishment of the first two extraembryonic cell lineages involved in implantation. Dev. Biol. *166*, 259–267.

Pan, D. (2007). Hippo signaling in organ size control. Genes Dev. *21*, 886–897.

Ralston, A., and Rossant, J. (2008). Cdx2 acts downstream of cell polarization to cell-autonomously promote trophectoderm fate in the early mouse embryo. Dev. Biol. *313*, 614–629.

Reddy, B.V., and Irvine, K.D. (2008). The Fat and Warts signaling pathways: new insights into their regulation, mechanism and conservation. Development *135*, 2827–2838.

Rossant, J., and Lis, W.T. (1979). Potential of isolated mouse inner cell masses to form trophectoderm derivatives in vivo. Dev. Biol. *70*, 255–261.

Sasaki, H., Nishizaki, Y., Hui, C., Nakafuku, M., and Kondoh, H. (1999). Regulation of Gli2 and Gli3 activities by an amino-terminal repression domain: implication of Gli2 and Gli3 as primary mediators of Shh signaling. Development (Cambridge, England) *126*, 3915–3924.

Saucedo, L.J., and Edgar, B.A. (2007). Filling out the Hippo pathway. Nat. Rev. Mol. Cell Biol. *8*, 613–621.

Sawada, A., Kiyonari, H., Ukita, K., Nishioka, N., Imuta, Y., and Sasaki, H. (2008). Redundant roles of Tead1 and Tead2 in notochord development and the regulation of cell proliferation and survival. Mol. Cell. Biol. *28*, 3177–3189.

Shirayoshi, Y., Okada, T.S., and Takeichi, M. (1983). The calcium-dependent cell-cell adhesion system regulates inner cell mass formation and cell surface polarization in early mouse development. Cell *35*, 631–638.

Silva, E., Tsatskis, Y., Gardano, L., Tapon, N., and McNeill, H. (2006). The tumor-suppressor gene fat controls tissue growth upstream of expanded in the hippo signaling pathway. Curr. Biol. *16*, 2081–2089.

Spindle, A.I. (1978). Trophoblast regeneration by inner cell masses isolated from cultured mouse embryos. J. Exp. Zool. *203*, 483–489.

St. John, M.A., Tao, W., Fei, X., Fukumoto, R., Carcangiu, M.L., Brownstein, D.G., Parlow, A.F., McGrath, J., and Xu, T. (1999). Mice deficient of Lats1 develop soft-tissue sarcomas, ovarian tumours and pituitary dysfunction. Nat. Genet. *21*, 182–186.

Strumpf, D., Mao, C.A., Yamanaka, Y., Ralston, A., Chawengsaksophak, K., Beck, F., and Rossant, J. (2005). Cdx2 is required for correct cell fate specification and differentiation of trophectoderm in the mouse blastocyst. Development *132*, 2093–2102.

Tanaka, S., Kunath, T., Hadjantonakis, A.K., Nagy, A., and Rossant, J. (1998). Promotion of trophoblast stem cell proliferation by FGF4. Science *282*, 2072–2075.

Tarkowski, A.K., and Wroblewska, J. (1967). Development of blastomeres of mouse eggs isolated at the 4- and 8-cell stage. J. Embryol. Exp. Morphol. *18*, 155–180.

Thompson, M., Andrade, V.A., Andrade, S.J., Pusl, T., Ortega, J.M., Goes, A.M., and Leite, M.F. (2003). Inhibition of the TEF/TEAD transcription factor activity by nuclear calcium and distinct kinase pathways. Biochem. Biophys. Res. Commun. *301*, 267–274.

Vassilev, A., Kaneko, K.J., Shu, H., Zhao, Y., and DePamphilis, M.L. (2001). TEAD/TEF transcription factors utilize the activation domain of YAP65, a Src/Yes-associated protein localized in the cytoplasm. Genes Dev. *15*, 1229–1241.

Willecke, M., Hamaratoglu, F., Kango-Singh, M., Udan, R., Chen, C.L., Tao, C., Zhang, X., and Halder, G. (2006). The fat cadherin acts through the hippo tumor-suppressor pathway to regulate tissue size. Curr. Biol. *16*, 2090–2100.

Wu, S., Liu, Y., Zheng, Y., Dong, J., and Pan, D. (2008). The TEAD/TEF family protein Scalloped mediates transcriptional output of the Hippo growth-regulatory pathway. Dev. Cell *14*, 388–398.

Yabuta, N., Okada, N., Ito, A., Hosomi, T., Nishihara, S., Sasayama, Y., Fujimori, A., Okuzaki, D., Zhao, H., Ikawa, M., et al. (2007). Lats2 is an essential mitotic regulator required for the coordination of cell division. J. Biol. Chem. *282*, 19259–19271.

Yagi, R., Kohn, M.J., Karavanova, I., Kaneko, K.J., Vullhorst, D., Depamphilis, M.L., and Buonanno, A. (2007). Transcription factor TEAD4 specifies the

trophectoderm lineage at the beginning of mammalian development. Development *134*, 3827–3836.

Yamagata, K., Yamazaki, T., Yamashita, M., Hara, Y., Ogonuki, N., and Ogura, A. (2005). Noninvasive visualization of molecular events in the mammalian zygote. Genesis *43*, 71–79.

Zhang, J., Smolen, G.A., and Haber, D.A. (2008a). Negative regulation of YAP by LATS1 underscores evolutionary conservation of the *Drosophila* Hippo pathway. Cancer Res. *68*, 2789–2794.

Zhang, L., Ren, F., Zhang, Q., Chen, Y., Wang, B., and Jiang, J. (2008b). The TEAD/TEF family of transcription factor Scalloped mediates Hippo signaling in organ size control. Dev. Cell *14*, 377–387.

Zhao, B., Wei, X., Li, W., Udan, R.S., Yang, Q., Kim, J., Xie, J., Ikenoue, T., Yu, J., Li, L., et al. (2007). Inactivation of YAP oncoprotein by the Hippo pathway is involved in cell contact inhibition and tissue growth control. Genes Dev. *21*, 2747–2761.

Zhao, B., Ye, X., Yu, J., Li, L., Li, W., Li, S., Yu, J., Lin, J.D., Wang, C.Y., Chinnaiyan, A.M., et al. (2008). TEAD mediates YAP-dependent gene induction and growth control. Genes Dev. *22*, 1962–1971.

A High-Speed Congenic Strategy Using First-Wave Male Germ Cells

Narumi Ogonuki[1], Kimiko Inoue[1,2], Michiko Hirose[1], Ikuo Miura[1], Keiji Mochida[1], Takahiro Sato[3,5], Nathan Mise[1], Kazuyuki Mekada[1], Atsushi Yoshiki[1], Kuniya Abe[1], Hiroki Kurihara[3], Shigeharu Wakana[1], Atsuo Ogura[1,2,4]*

1 RIKEN BioResource Center, Tsukuba, Ibaraki, Japan, **2** Graduate School of Life and Environmental Science, University of Tsukuba, Tsukuba, Ibaraki, Japan, **3** Department of Physiological Chemistry and Metabolism, Graduate School of Medicine, The University of Tokyo, Bunkyo-ku, Tokyo, Japan, **4** Center for Disease Biology and Integrative Medicine, Graduate School of Medicine, The University of Tokyo, Bunkyo-ku, Tokyo, Japan, **5** Tsukuba Safety Assessment Laboratories, Banyu Pharmaceutical Company Limited, Tsukuba, Ibaraki, Japan

Abstract

Background: In laboratory mice and rats, congenic breeding is essential for analyzing the genes of interest on specific genetic backgrounds and for analyzing quantitative trait loci. However, in theory it takes about 3–4 years to achieve a strain carrying about 99% of the recipient genome at the tenth backcrossing (N10). Even with marker-assisted selection, the so-called 'speed congenic strategy', it takes more than a year at N4 or N5.

Methodology/Principal Findings: Here we describe a new high-speed congenic system using round spermatids retrieved from immature males (22–25 days of age). We applied the technique to three genetically modified strains of mice: transgenic (TG), knockin (KI) and *N*-ethyl-*N*-nitrosourea (ENU)-induced mutants. The donor mice had mixed genetic backgrounds of C57BL/6 (B6):DBA/2 or B6:129 strains. At each generation, males used for backcrossing were selected based on polymorphic marker analysis and their round spermatids were injected into B6 strain oocytes. Backcrossing was repeated until N4 or N5. For the TG and ENU-mutant strains, the N5 generation was achieved on days 188 and 190 and the proportion of B6-homozygous loci was 100% (74 markers) and 97.7% (172/176 markers), respectively. For the KI strain, N4 was achieved on day 151, all the 86 markers being B6-homozygous as early as on day 106 at N3. The carrier males at the final generation were all fertile and propagated the modified genes. Thus, three congenic strains were established through rapid generation turnover between 41 and 44 days.

Conclusions/Significance: This new high-speed breeding strategy enables us to produce congenic strains within about half a year. It should provide the fastest protocol for precise definition of the phenotypic effects of genes of interest on desired genetic backgrounds.

Citation: Ogonuki N, Inoue K, Hirose M, Miura I, Mochida K, et al. (2009) A High-Speed Congenic Strategy Using First-Wave Male Germ Cells. PLoS ONE 4(3): e4943. doi:10.1371/journal.pone.0004943

Editor: Simon Melov, Buck Institute for Age Research, United States of America

Received December 11, 2008; **Accepted** February 19, 2009; **Published** March 31, 2009

Funding: This work was supported by KAKENHI (20062012 [A.O.] and 19300151 [A.O.]). The funders had no role in study design, data collection and analysis, decision to publish, or preparation of the manuscript.

Competing Interests: The authors have declared that no competing interests exist.

* E-mail: ogura@rtc.riken.go.jp

Introduction

For nearly 30 years, the genetic manipulation of laboratory mice has contributed substantially to the development of many fields in medical research and mammalian biology. Remarkably, by genetically altering the mouse genome with single nucleotide precision, it is now possible to create mice with desired genetic modifications to assess gene function in healthy animals and in animal models for human diseases. One major issue associated with mouse genetic engineering is that the biological function of engineered genes can vary with their genetic background [1–3]. This often raises serious concerns, because transgenic (TG) or knockout (or knockin, KI) mice are generated in strains that have historically been selected for the ease and convenience of generating the TG or knockout strain, rather than phenotypic characterization of the mutation itself. For example, most embryonic stem (ES) cell lines used for knockout experiments are derived from the 129 strain. Unfortunately, however, this strain has significant biological limitations that interfere with the phenotypic analysis of a target mutation. It consists of a diverse and complex family of substrains [4] and many of these have an atypical brain structure [5]. Therefore, for facilitating definition of transgene or gene-targeted effects over a given genetic background, the engineered gene should be introduced from the donor strain into the desired recipient strain.

The classical protocol for such purpose is congenic breeding: serially backcrossing the gene donor to the recipient strain accompanied by selection for progeny carrying the desired gene in each backcross generation. This protocol calls for 10 backcross generations (N10), followed by an intercross (F1) to produce founders that are homozygous for the desired gene (theoretically more than 99% of the genome) [6]. Although the strategy is

simple, the process is expensive and time consuming, requiring roughly 3–4 years to produce any given congenic strain. To overcome this weakness, reduction of backcross generations for the establishment of congenic strains has been achieved using marker-assisted selection protocols (MASP), the so-called 'speed congenics'. The time required for deriving such congenic strains is about 1–2 years, depending on the robustness and intensiveness of the polymorphic analysis between the gene donor and recipient strains [7].

One interesting suggestion is that the breeding cycle could be shortened by superovulating and breeding juvenile females (3–4 weeks) followed by embryo transfer to mature females for production of the next generation [8]. This might shorten the generation time down to 6–7 weeks and reduce the whole congenic procedure to 1 year. This 'supersonic congenics' strategy was promising, but has not proved practical because of the limited number of oocytes that can be produced and because there are great individual differences in response to superovulation resumes.

We have attempted to develop another high-speed congenic strategy through the male germline. Recently, we have shown that the genomes of male germ cells from the first wave of spermatogenesis have the ability to support embryonic development to term. Mouse round spermatids—the youngest haploid male germ cells—appear first at 17 days after birth and can be used for the production of offspring by round spermatid injection (ROSI) into oocytes [9]. We applied this technique to the generation of congenic strains from mice with mixed genotypes bearing a transgene, a targeted KI gene or chemically induced mutant genes. At each generation, males used for backcrossing were selected based on polymorphic marker analysis: low density screening MASP using 74–176 markers distributed uniformly throughout the genome. The recipient strain for the expected genetic background was C57BL/6 for all lines of congenics. The results were very consistent and the time for producing a congenic strain was reduced significantly. Therefore, our high-speed congenic system would be very useful for the accelerated analysis of genes of interest under a defined genetic background.

Results and Discussion

Definition of the optimal male age for spermatid collection

In mice, round spermatids can be collected from 17-day-old males at the earliest and their genomes can support full term embryonic development after injection into oocytes using ROSI [9]. However, the efficiency of producing offspring using these round spermatids was extremely low (0.9%) because of their very low incidence in testicular cell suspensions (<2%). This might compromise the accurate identification of round spermatids within a limited time of oocyte micromanipulation. Therefore, we first checked the proportion of round spermatids in testicular cell suspensions from males aged 18, 20, 22 and 24 days to define the optimal age for applying ROSI. As shown in Figure 1, the percentages of round spermatids in testicular suspension increased consistently from days 18 to 24 with statistically significant differences between groups ($P<0.05$). This resulted in easier identification of round spermatids under a microscope: thus, the time required for picking up a single round spermatid was roughly 60, 15, 10 and 10 sec using cell suspensions collected at days 18, 20, 22 and 24, respectively. Therefore, we defined day 22 to be the earliest age of males that allowed the efficient identification of round spermatids in testicular cell suspensions. Testes of the mice at day 22 were smaller than in adults, but we could still collect sufficient round spermatids from a single testis to perform a ROSI experiment (about 150–250 injected oocytes).

Congenics of gene-modified strains using first-wave round spermatids

To test whether high-speed congenics using the first wave of round spermatids could be used practically, we applied the technique to three different types of gene-modified strains, TG, KI and *N*-ethyl-*N*-nitrosourea (ENU)-mutant strains. At each generation, a male used for the next application of ROSI was selected based on showing fewer heterozygous alleles by polymorphic markers that could identify the donor (DBA/2 and 129) and

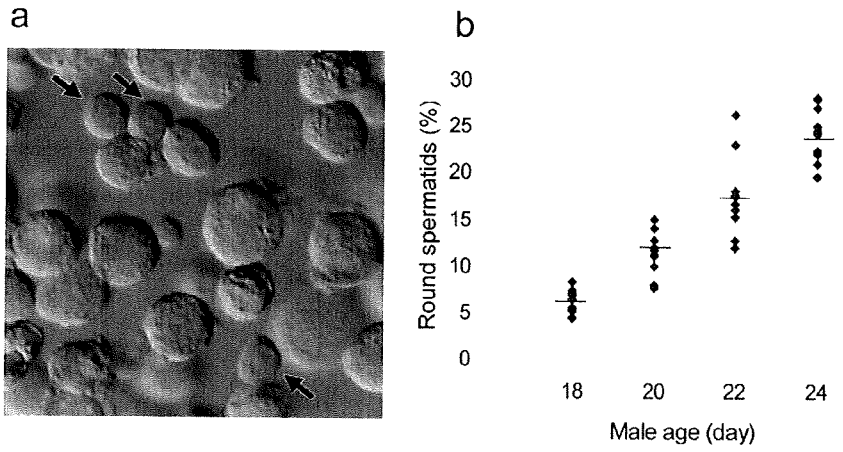

Figure 1. Definition of the optimal male age for spermatid collection. a) Representative photomicrograph of a cell suspension prepared from the testis of a male mouse at 24 days of age. Arrows indicate round spermatids, which are easily identified by a round nucleus and a high cytoplasmic/nuclear ratio. b) The proportion of round spermatids among testicular cells from 18 days to 24 days after birth. The percentages of round spermatids in testicular suspension increased consistently from days 18 to 24 ($P<0.05$ between groups). The cells were counted in two different males by two different operators. The horizontal bars indicate the average.
doi:10.1371/journal.pone.0004943.g001

recipient strains (B6Cr and B6J). Backcross ROSI was repeated until the N4 or N5 generation. After this, additional backcrossing was continued by natural mating to reduce the undetected gaps of contaminating donor alleles [10].

The *Vasa Venus* TG strain we used was generated from embryos produced by IVF using (B6Cr×DBA/2)F1 strain oocytes and B6Cr strain spermatozoa, and maintained by full-sib mating. The N1 offspring were obtained by ICSI using a donor male at F7. As shown in Figure 2a, N5 backcross offspring were obtained on day 188 and all 74 markers were identified as B6 homozygous in one of two carrier males.

The $Ednra^{EGFP/+}$ KI strain was derived from ES cells with a (B6Cr×129^{+Ter}/SvJcl)F1 genetic background [11]. The first N1 generation was obtained by IVF using B6Cr oocytes and spermatozoa from a chimeric mouse. All 86 markers were homozygous for B6Cr as early as at N3 (day 106; 2 out of 14 carrier males) and N4 offspring were obtained on day 151 (Figure 2b).

The ENU-induced growth differentiation factor 5 (*Gdf5*) mutant line had a mixed genetic background of B6J and DBA/2J [12]. For this combination of inbred strains, more dense polymorphic markers were available using single nucleotide polymorphism (SNP) assays as well as microsatellite genotyping (176 markers; see Materials and Methods). The N5 generation was obtained on day 190 and was 97.7% (172/176) homozygous for B6J (Figure 2c). The following N6 and N7 generations produced by IVF were 98.8% and 99.4% homozygous for B6J, respectively.

The efficiency rates in backcross breeding by ROSI in these gene-modified strains are shown in Table 1. All the modified genes could be propagated successfully into the next generations by ROSI. The male carriers finally obtained were all fertile and propagated the modified genes to the next generation by natural mating.

Significance of congenic breeding using first-wave male germ cells

Congenic strains have been used extensively for the study of mouse genetics including definition of phenotypic effects of genes on specific genetic backgrounds and identification of genes or genomic segments affecting the phenotypes of interest by quantitative trait locus (QTL) analysis. However, it takes about 2–3 years to construct a congenic strain with a level of genetic homogeneity that is reliable for research (>99% or more) [6]. To accelerate congenic breeding, MASP has been developed by taking advantage of precise information on mouse genetics [7]. Another approach for efficient congenics should be rapid generation turnover by assisted reproduction techniques. The use of immature females proposed by Behringer [8] was applied

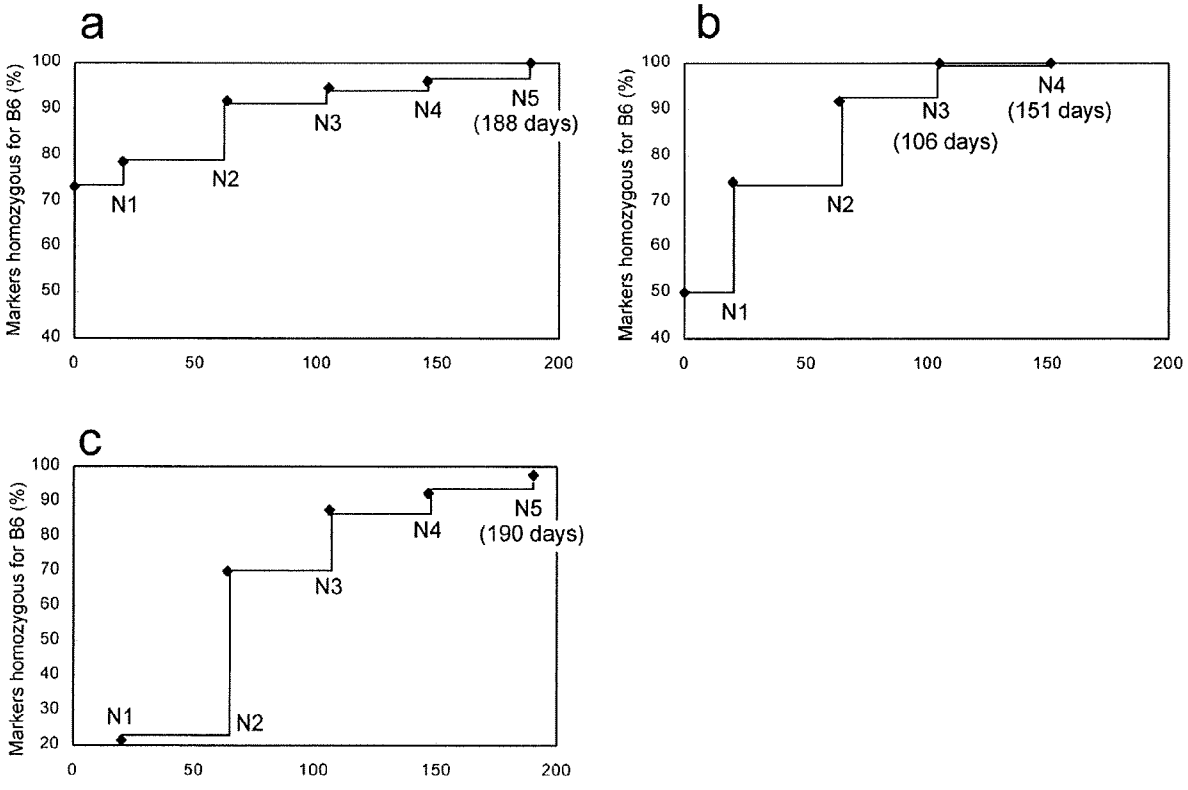

Figure 2. Time course of generation turnover and the rate of markers homozygous for the C57BL/6 (B6) type. a) *Vasa–Venus* transgenic strain. All markers (n = 74) were homozygous for B6 at N5 on day 188. b) $Ednra^{EGFP/+}$ knockin strain. All markers (n = 86) were homozygous for B6 at N3 on day 106 and N4 offspring were obtained on day 151. c) ENU-induced *Gdf5* mutant strain. The N5 generation was obtained on day 190 and was 97.7% (172/176) homozygous for B6. There were 74, 86 and 176 polymorphic markers, which identified the alleles for the C57BL/6Cr:DBA/2Cr, C57BL/6Cr:129 and C57BL/6J:DBA/2J strains, respectively. Each generation turnover was between 42 and 45 days: the age of the donor male plus the gestation period (20 days) minus the one-day overlap between them.
doi:10.1371/journal.pone.0004943.g002

Table 1. Results of congenic breeding by round spermatid injection (ROSI) in three gene-modified strains.

Strain	Generation produced	Age (day) of male used for ROSI	No. of oocyes that survived ROSI	No. (%) of oocytes that developed to 2-cells	No. of 2-cells transferred	No. (%) implanted	No. (%) born	No. (%) of males born	No. (%) of male carriers
Vasa-Venus transgenic	N1	Adult (ICSI)	16	15 (93.8)	15	10 (66.7)	5 (33.3)	5 (33.3)	5 (33.3)*
	N2	24	182	164 (90.1)	164	69 (42.1)	24 (14.6)	12 (7.3)	4 (2.4)
	N3	23	123	109 (88.6)	109	24 (22.0)	4 (3.7)	2 (1.8)	1 (0.9)
	N4	22	172	156 (90.7)	156	51 (32.7)	14 (9.0)	6 (3.8)	2 (1.3)
	N5	23	134	123 (91.8)	123	23 (18.7)	10 (8.1)	4 (3.3)	2 (1.6)
Ednra-EGFP knockin**	N1	Adult (IVF)	166	135 (81.3)	135	62 (45.9)	49 (36.3)	23 (17.0)	12 (8.9)
	N2	24	243	196 (80.7)	196	63 (32.1)	30 (15.3)	10 (5.1)	5 (2.6)
	N3	24	261	235 (90.0)	235	107 (45.5)	52 (22.1)	30 (12.8)	14 (6.0)
	N4	25	244	215 (88.1)	215	72 (33.5)	39 (18.1)	19 (8.8)	11 (5.1)
ENU-induced mutant	N1	Adult (IVF)	80	49 (61.3)	49	Not observed	26 (53.1)	14 (28.6)	3 (6.1)
	N2	25	201	158 (78.6)	158	54 (34.2)	25 (15.8)	11 (7.0)	4 (2.5)
	N3	23	208	194 (93.3)	194	68 (35.1)	26 (13.4)	12 (6.2)	7 (3.6)
	N4	22	173	127 (73.4)	127	51 (40.2)	13 (10.2)	5 (3.9)	2 (1.6)
	N5	24	216	177 (81.9)	177	91 (51.4)	34 (19.2)	10 (5.6)	4 (2.3)
Total (ROSI only)			2157	1854 (86.0)	1854	673 (36.3)	271 (14.6)	121 (6.5)	56 (3.0)
Control (C57BL/6)		22–24	467	349 (74.7)	329	133 (40.4)	49 (14.9)	26 (7.9)	

*The implantation sites were identified as the scars of decidualization at caesarian section.
**The donor male (N0) was homozygous for the transgene.
***All genetic markers tested were homozygous for the B6 mouse strain at N3.
doi:10.1371/journal.pone.0004943.t001

successfully to the derivation of a conplastic strain of rats [13]. However, there have been very few similar applications published, probably because of the limited number of oocytes produced from any one female, which may attenuate the number of carrier females in the subsequent generations. Our high-speed congenic system uses immature males as founders at each generation. Unlike females, each male can produce a large number of germ cells and multiple litters of offspring. This not only assures the safe propagation of the target gene on to the next generation, but also enables efficient selection of a male for the next round of ROSI, thus significantly shortening the time for congenics.

In this study, the advantages of our high-speed congenic strategy were shown in the KI strain, which started with a (B6Cr×129)F1 genetic background: all 86 markers were homozygous for the B6 strain as early as 106 days (N3). Apparently, it is more straightforward to use B6 ES cells for gene targeting if the B6 genetic background is required. Several B6 ES cells are available for gene targeting [14,15], and the International Knockout Consortium uses C57BL/6 ES cell lines [16]. However, B6 ES cells usually require more intense care than other 129 or hybrid ES cells to maintain their germline transmission ability during gene targeting. ES cells with hybrid genetic constitutions of B6 and 129 are easy to maintain and can be used efficiently for producing gene-targeted offspring [1,11], especially by tetraploid complementation [17]. If the gene-targeted allele is of B6 origin, it may avoid the persistence of donor genetic segments around the targeted allele during congenic production, which inevitably occurs when 129 ES cells are used. Thus, the combination of gene-targeting (B6×129)F1 ES cells and the new high-speed congenic breeding may be an alternative fast protocol to generate a B6 gene-targeting strain.

A congenic breeding strategy has also been employed extensively in laboratory rats because it is now possible to map the genetic variants and mutations that underlie complex disease-related phenotypes in this species [18,19]. ROSI is successful in some, but not all, strains of rats [20]. As the first wave of round spermatids appears in rat testes around 26 days after birth, we estimate that congenic rat strains could be generated within 7 or 8 months by using these germ cells [21].

We anticipate that the congenic strategy developed in this study might be accelerated further using male germ cells that are younger than round spermatids. This is possible theoretically, because the genomes of primary spermatocytes—premeiotic male germ cells—can support the full term development of embryos [22]. Despite many efforts to improve the technique, however, the efficiency of producing offspring using primary spermatocytes is very low [22,23]. Therefore, at present the use of round spermatids on days 22–25 may be the most practical range for efficient, rapid backcross breeding in mice. As far as we know, this is the most rapid generational turnover by sexual reproduction in mammals.

Technical issues associated with congenics by ROSI

As mentioned above, the high-speed congenic strategy we developed is very promising to produce congenic strains with desired genetic backgrounds. One of the technical issues associated with this strategy is that ROSI needs some skill and experience. However, ROSI is generally easier to perform than conventional ICSI because of the high survival rate of oocytes after injection: the diameter of injection pipettes is small and the activated oocytes used for ROSI are more resistant to the injection stimulus than nonactivated oocytes [24]. From our experience, training of three

to four consecutive weeks is enough for ROSI if the operator already has the basic technique for embryo handling. For ICSI, reliable protocol papers are available [25,26] and the same protocols can be essentially applied to ROSI. Oocytes from B6 females tend to be more sensitive to injection than those from other strains, but this problem might be overcome by using a high osmotic strength medium for manipulation on the microscope stage, if necessary. In our ROSI experiments using B6 oocytes, about 80% survived the injection whereas about 90% survived in other strains including B6D2F1, DBA/2 and 129 (unpublished).

As shown in Table 1, we consistently obtained sufficient carrier males for selection except for the N3 to N5 generations in the *Vasa-Venus* TG strain, which were affected by an accidental decline in the quality of recipient females, for reasons unknown. Based on the overall efficiency in our ROSI experiments presented in Table 1, we estimated the number of oocytes to be injected with the aim of obtaining expected number of carrier males (Table 2). These numbers of oocytes can be handled by one or two operators in a single session.

One can question if epigenetic modifications might have occurred during conception using round spermatids, because ROSI-derived preimplantation embryos have shown some disturbances in gene expression [27,28] and aberrant DNA methylation [29]. However, epigenetic errors imposed on individuals are normally erased during germ cell development and are never transmitted to the next generation by natural mating, as shown in mouse somatic cell cloning experiments [30,31]. Therefore, once mated naturally, congenic strains produced by ROSI are expected to become epigenetically indistinguishable from those produced by conventional congenic protocols.

Conclusions

The generation turnover time in mice can be shortened to about 40 days by using the first wave round spermatids as male gametes. We confirmed that this breeding strategy reduced the time required for congenesis to about half a year. This should provide the earliest opportunities for the analysis of genes of interest under a defined genetic background and for QTL mapping, which are becoming integral to biomedical research using the mouse as a model.

Materials and Methods

The origin of donor strains

The B6 substrains used in this study were B6Cr (C57BL/6CrSlc) and B6J (C57BL/6JJcl), which were purchased from CLEA Japan, Inc. (Kanagawa) and Japan SLC, Inc. (Shizuoka), respectively [32]. One mature male mouse from each strain was used as the donor of the modified gene. The TG strain we used was Tg(Mvh-Venus)1Rbrc, which was generated by DNA nuclear injection into zygotes derived from IVF using (B6Cr×DBA/2)F1 oocytes and B6Cr spermatozoa. The *Mvh-Venus* gene clearly shows the germline origin of living cells by green fluorescence because of the highly specific expression of the *Mvh* (mouse vasa homologue) gene [33]. The strain was maintained by full-sib mating. An F7 male homozygous for the transgene was used as the donor.

The KI line we used was the $Ednra^{EGFP/+}$ strain carrying the reporter gene for enhanced green fluorescence protein (EGFP) that had been knocked into the *Ednra* (endothelin receptor type A) locus by recombinase-mediated cassette exchange based on the Cre-lox system [11]. The gene-targeted ES cells had the (B6Cr×129^{+Ter}/SvJcl)F1 genotype. Chimeric embryos were produced by injection of ES cells into ICR blastocysts and they were transferred into pseudopregnant ICR females. A chimeric male thus obtained were used for producing N1 by conventional IVF using B6Cr oocytes.

The ENU-induced mutant strain we used carried a point mutation at the *Gdf5* locus. This mutation causes an amino acid substitution in a highly conserved region of the active signaling domain of the GDF5 (growth differentiation factor 5) protein, leading to impaired joint formation and osteoarthritis [12]. The donor male had a mixed genetic background of B6J and DBA/2 because the strain was generated from a cross of an ENU-mutagenized B6J male and a wild-type DBA/2 female.

Offspring that carried modified genes were genotyped at each generation by polymerase chain reaction (PCR) amplification with specific primers for the given TG strain [34], by specific green fluorescence over the body for the KI strain and by PCR-based sequencing for the ENU mutant strain [12].

Table 2. The numbers of superovulated females and oocytes required for obtaining selectable numbers of carrier males, as estimated from the data in Table 1.

Females superovulated (25–30 oocytes per female)	4 to 5	6 to 7	7 to 8
Oocytes injected	125	167	208
Oocytes survived (80% per oocytes injected)	100	133	167
2-cells transferred (80% per oocytes survived)	80	107	133
Birth (15% per 2-cells transferred)	12	16	20
Males (50% per birth)	6	8	10
Carrier males (50% per males)	3	4	5

doi:10.1371/journal.pone.0004943.t002

Collection of oocytes

Female B6Cr or B6J strain mice (7–10 weeks old) were each injected with 7.5 units of equine chorionic gonadotropin followed by injection of 7.5 units of human chorionic gonadotropin (hCG) 48 h later. Mature oocytes were collected from the oviducts 15–17 h after hCG injection and were freed from cumulus cells by treatment with 0.1% hyaluronidase in CZB medium [35]. The oocytes were transferred to fresh CZB medium and incubated at 37°C in an atmosphere of 5% CO_2 in air for up to 90 min before ROSI.

Preparation of testicular cell suspensions

Spermatogenic cells were prepared mechanically as described for hamsters [36]. Briefly, testes were removed from 18- to 25-day-old males and placed in erythrocyte-lysing buffer (155 mM NH_4Cl/10 mM $KHCO_3$/2 mM EDTA, pH 7.2). For the first series of experiments to identify the optimal age of males for donors, we used ICR males; as far as we examined there were no strain-dependent differences in the timing of the first wave of spermatogenesis. The tunica albuginea was removed and the seminiferous tubule masses were transferred into cold (4°C) Dulbecco's phosphate buffered saline (PBS) supplemented with 5.6 mM glucose, 5.4 mM sodium lactate and 0.1 mg/ml of polyvinyl alcohol (polyvinylpyrrolidone, PVP, in the original report) (GL-PBS) [36]. The seminiferous tubules were cut into small pieces and pipetted gently to disperse spermatogenic cells into the GL-PBS. Then, the cell suspension was filtered through a 38-μm nylon mesh and washed three times by centrifugation (200 *g* for 4 min). To define the optimal male age for spermatid collection, we first examined the proportion of round spermatids in

cell suspensions collected from two males aged at 18, 20, 22, or 24 days. The percentages of round spermatids were analyzed using arcsine transformation, followed by one-way ANOVA analysis and a *post-hoc* procedure using Scheffe's test for multiple comparisons.

ROSI

ROSI was performed using a Piezo-driven micromanipulator (Prime Tech Ltd., Ibaraki, Japan) as described [37,38]. The cover of a plastic dish (Falcon no. 1006; Becton Dickinson, Franklin Lakes, NJ) was used as a microinjection chamber. Several small drops (~4 μl) of Hepes-buffered CZB with or without 10% PVP were placed on the bottom and covered with mineral oil. Spermatogenic cells were placed in one of the PVP droplets. Before injection of the nuclei of round spermatids, oocytes were activated by treatment with Ca^{2+}-free CZB medium containing 2.5 mM $SrCl_2$ for 20 min at 37°C. Oocytes reaching telophase II at 40–90 min after onset of activation treatment were each injected with a round spermatid. They were kept in Hepes-CZB at room temperature (24°C) for ~10 min before culture in CZB at 37°C under 5% CO_2 in air.

Embryo culture and transfer

Embryos that reached the 2-cell stage by 24 h of culture in CZB were transferred into the oviducts of pseudopregnant ICR strain females (8–12 weeks old) on the day after mating (day 0.5). On day 19.5, recipient females were killed and their uteri were examined for live term fetuses. These were nursed by lactating ICR foster females. The day of birth was designated day 0.5 for newborns.

Care and use of animals

All procedures described here were reviewed and approved by the Animal Experimental Committee at the RIKEN Institute.

Genotyping for MASP

Tail clips about 0.3 cm long were collected for DNA extraction, using the Wizard Genomic DNA Purification Kit (Promega, Madison, WI) and the DNeasy 96 Blood & Tissue Kit (#69582; QIAGEN GmbH, Hilden, Germany) according to the manufacturers' instructions. Microsatellite genotyping was carried out by PCR for simple sequence length polymorphisms (SSLP) using microsatellite markers. The microsatellite markers were selected out of sequence length polymorphisms between B6 and DBA/2 and B6 and 129 strains (Mekada et al., unpublished data) (Tables S1 and S2). PCR execution was performed using the QIAGEN Multiplex PCR kit (#206143; QIAGEN GmbH) and the length polymorphism was detected by agarose gel electrophoresis. Map locations and primer sequences of the microsatellite loci were used according to the Mouse Genome Informatics (MGI) of the Jackson Laboratory, USA, and Mouse Microsatellite Data Base of Japan (MMDBJ).

SNP genotyping was carried out using a TaqMan Minor Groove Binding (MGB) assay (Applied Biosystems, Foster City, CA). TaqMan MGB probe sets were designed based on SNP polymorphism between C57BL/6J and DBA/2J (Table S3). PCR execution was performed using TaqMan Genotyping Master Mix (#4371353; Applied Biosystems). SNP polymorphisms were detected using an ABI PRISM 7900HT Sequence Detection System (Applied Biosystems).

Supporting Information

Table S1 Variation alleles between C57BL/6 and DBA/2 mouse strains.
Found at: doi:10.1371/journal.pone.0004943.s001 (0.02 MB XLS)

Table S2 Variation alleles between C57BL/6 and 129 mouse strains.
Found at: doi:10.1371/journal.pone.0004943.s002 (0.02 MB XLS)

Table S3 The SNPs information that designed the TaqMan MGB probe sets.
Found at: doi:10.1371/journal.pone.0004943.s003 (0.02 MB XLS)

Acknowledgments

We would like to thank Drs. Masumi Hirabayashi and Hiromi Miki for discussion on round spermatid injection techniques and Dr. Tomokazu Amano for the genetic information on the (B6×129)F1 ES cell line.

Author Contributions

Conceived and designed the experiments: NO AO. Performed the experiments: NO KI MH IM KM KM. Analyzed the data: NO IM SW AO. Contributed reagents/materials/analysis tools: TS NM KM AY KA YK. Wrote the paper: NO IM SW AO.

References

1. Glaser S, Anastassiadis K, Stewart AF (2005) Current issues in mouse genome engineering. Nat Genet 37: 1187–1193.
2. Yoshiki A, Moriwaki K (2006) Mouse phenome research: implications of genetic background. ILAR J 47: 94–102.
3. Eisener Dorman AF, Lawrence DA, Bolivar VJ (2008) Cautionary insights on knockout mouse studies: The gene or not the gene? Brain Behav Immun, In press.
4. Simpson EM, Linder CC, Sargent EE, Davisson MT, Mobraaten LE, et al. (1997) Genetic variation among 129 substrains and its importance for targeted mutagenesis in mice. Nat Genet 16: 19–27.
5. Livy DJ, Wahlsten D (1991) Tests of genetic allelism between four inbred mouse strains with absent corpus callosum. J Hered 82: 459–464.
6. Flaherty L (1981) Congenic strains. In: Foster HL, Small JD, Fox JG, eds. The Mouse in Biomedical Research (Vol. 1). New York: Academic Press. pp 215–222.
7. Markel P, Shu P, Ebeling C, Carlson GA, Nagle DL, et al. (1997) Theoretical and empirical issues for marker-assisted breeding of congenic mouse strains. Nat Genet 17: 280–284.
8. Behringer R (1998) Supersonic congenics? Nat Genet 18: 108.
9. Miki H, Lee J, Inoue K, Ogonuki N, Noguchi Y, et al. (2004) Microinsemination with first-wave round spermatids from immature male mice. J Reprod Dev 50: 131–137.
10. Armstrong NJ, Brodnicki TC, Speed TP (2006) Mind the gap: analysis of marker-assisted breeding strategies for inbred mouse strains. Mamm Genome 17: 273–287.
11. Sato T, Kawamura Y, Asai R, Amano T, Uchijima Y, et al. (2008) Recombinase-mediated cassette exchange reveals the selective use of Gq/G11-dependent and -independent endothelin 1/endothelin type A receptor signaling in pharyngeal arch development. Development 135: 755–765.
12. Masuya H, Nishida K, Furuichi T, Toki H, Nishimura G, et al. (2007) A novel dominant-negative mutation in Gdf5 generated by ENU mutagenesis impairs joint formation and causes osteoarthritis in mice. Hum Mol Genet 16: 2366–2375.
13. Pravenec M, Hyakukoku M, Houstek J, Zidek V, Landa V, et al. (2007) Direct linkage of mitochondrial genome variation to risk factors for type 2 diabetes in conplastic strains. Genome Res 17: 1319–1326.
14. Seong E, Saunders TL, Stewart CL, Burmeister M (2004) To knockout in 129 or in C57BL/6: that is the question. Trends Genet 20: 59–62.
15. Pacholczyk G, Suhag R, Mazurek M, Dederscheck SM, Koni PA (2008) Generation of C57BL/6 knockout mice using C3H×BALB/c blastocysts. Biotechniques 44: 413–416.
16. Collins FS, Rossant J, Wurst W (2007) A mouse for all reasons. Cell 128: 9–13.
17. George SH, Gertsenstein M, Vintersten K, Korets Smith E, Murphy J, Stevens ME, Haigh JJ, Nagy A (2007) Developmental and adult phenotyping

directly from mutant embryonic stem cells. Proc Natl Acad Sci U S A 104: 4455–4460.
18. Aitman TJ, Critser JK, Cuppen E, Dominiczak A, Fernandez-Suarez XM, et al. (2008) Progress and prospects in rat genetics: a community view. Nat Genet 40: 516–522.
19. Saar K, Beck A, Bihoreau MT, Birney E, Brocklebank D, et al. (2008) SNP and haplotype mapping for genetic analysis in the rat. Nat Genet 40: 560–566.
20. Hirabayashi M, Kato M, Aoto T, Ueda M, Hochi S (2002) Rescue of infertile transgenic rat lines by intracytoplasmic injection of cryopreserved round spermatids. Mol Reprod Dev 62: 295–299.
21. Jahnukainen K, Chrysis D, Hou M, Parvinen M, Eksborg S, et al. (2004) Increased apoptosis occurring during the first wave of spermatogenesis is stage-specific and primarily affects midpachytene spermatocytes in the rat testis. Biol Reprod 70: 290–296.
22. Ogura A, Suzuki O, Tanemura K, Mochida K, Kobayashi Y, et al. (1998) Development of normal mice from metaphase I oocytes fertilized with primary spermatocytes. Proc Natl Acad Sci U S A 95: 5611–5615.
23. Miki H, Ogonuki N, Inoue K, Baba T, Ogura A (2006) Improvement of cumulus-free oocyte maturation in vitro and its application to microinsemination with primary spermatocytes in mice. J Reprod Dev 52: 239–248.
24. Miki H, Hirose M, Ogonuki N, Inoue K, Kezuka F, et al. Efficient production of androgenetic embryos by round spermatid injection. Genesis, In press.
25. Nagy A, Gertsenstein M, Vintersten K, Behringer R (2003) Manipulating the Mouse Embryo: A Laboratory Manual (3rd edition). New York: Cold Spring Harbor Laboratory Press. 565 p.
26. Yoshida N, Perry AC (2007) Piezo-actuated mouse intracytoplasmic sperm injection (ICSI). Nat Protoc 2: 296–304.
27. Hayashi S, Yang J, Christenson L, Yanagimachi R, Hecht NB (2003) Mouse preimplantation embryos developed from oocytes injected with round spermatids or spermatozoa have similar but distinct patterns of early messenger RNA expression. Biol Reprod 69: 1170–1176.
28. Ziyyat A, Lefevre A (2001) Differential gene expression in pre-implantation embryos from mouse oocytes injected with round spermatids or spermatozoa. Hum Reprod 16: 1449–1456.
29. Kishigami S, Van Thuan N, Hikichi T, Ohta H, Wakayama S, et al. (2006) Epigenetic abnormalities of the mouse paternal zygotic genome associated with microinsemination of round spermatids. Dev Biol 289: 195–205.
30. Shimozawa N, Ono Y, Kimoto S, Hioki K, Araki Y, et al. (2002) Abnormalities in cloned mice are not transmitted to the progeny. Genesis 34: 203–207.
31. Tamashiro KLK, Wakayama T, Akutsu H, Yamazaki Y, Lachey JL, et al. (2002) Cloned mice have an obese phenotype not transmitted to their offspring. Nat Med 8: 262–267.
32. Mekada K, Abe K, Murakami A, Nakamura S, Nakata H, Moriwaki K, Obata Y, Yoshiki A (2009) Genetic differences among C57BL/6 substrains. Exp Anim, In press.
33. Fujiwara Y, Komiya T, Kawabata H, Sato M, Fujimoto H, et al. (1994) Isolation of a DEAD-family protein gene that encodes a murine homolog of Drosophila vasa and its specific expression in germ cell lineage. Proc Natl Acad Sci U S A 91: 12258–12262.
34. Nagai T, Ibata K, Park ES, Kubota M, Mikoshiba K, et al. (2002) A variant of yellow fluorescent protein with fast and efficient maturation for cell-biological applications. Nat Biotechnol 20: 87–90.
35. Chatot CL, Ziomek CA, Bavister BD, Lewis JL, Torres I (1989) An improved culture medium supports development of random-bred 1-cell mouse embryos in vitro. J Reprod Fertil 86: 679–688.
36. Ogura A, Yanagimachi R (1993) Round spermatid nuclei injected into hamster oocytes form pronuclei and participate in syngamy. Biol Reprod 48: 219–225.
37. Kimura Y, Yanagimachi R (1995) Mouse oocytes injected with testicular spermatozoa or round spermatids can develop into normal offspring. Development 121: 2397–2405.
38. Ogonuki N, Mochida K, Miki H, Inoue K, Fray M, et al. (2006) Spermatozoa and spermatids retrieved from frozen reproductive organs or frozen whole bodies of male mice can produce normal offspring. Proc Natl Acad Sci U S A 103: 13098–13103.

Stimulation of sensory neurons improves cognitive function by promoting the hippocampal production of insulin-like growth factor-I in mice

NAOAKI HARADA, NORIKO NARIMATSU, HIROKI KURIHARA, NAOMI NAKAGATA, and KENJI OKAJIMA

NAGOYA, TOKYO, AND KUMAMOTO, JAPAN

Calcitonin gene-related peptide (CGRP) increases the production of insulin-like growth factor-I (IGF-I) in the mouse brain. IGF-I exerts beneficial effects on the cognitive function by increasing synaptic transmission and by inducing angiogenesis and neurogenesis in the hippocampus. In the current study, we examined whether stimulation of sensory neurons by capsaicin improved the cognitive function by increasing the production of IGF-I in the hippocampus using wild-type (WT) and CGRP-knockout (CGRP−/−) mice.

Significant increases of the hippocampal tissue levels of CGRP, IGF-I, and IGF-I messenger RNA (mRNA) were observed after capsaicin administration in WT mice ($P < 0.01$) but not in CGRP−/− mice. Increase in the expression of *c-fos* was also observed in the spinal dorsal horn, the parabrachial nuclei, and the hippocampus after capsaicin administration in WT mice but not in CGRP−/− mice. Significant enhancement of angiogenesis and neurogenesis was observed in the dentate gyrus of the hippocampus after capsaicin administration in WT mice ($P < 0.01$) but not in CGRP−/− mice. Although capsaicin administration improved spatial learning in WT mice, no such effect was observed in CGRP−/− mice. Capsaicin-induced improvement of the spatial learning was reversed by administration of an anti-IGF-I antibody and by that of a CGRP receptor antagonist CGRP (8-37) in WT mice. The administration of IGF-I improved the spatial learning in both WT and CGRP−/− mice. These observations strongly suggest that the stimulation of sensory neurons by capsaicin might increase IGF-I production via increasing the hippocampal tissue CGRP levels, and it may thereby promote angiogenesis and neurogenesis to produce improvement of the cognitive function in mice. (Translational Research 2009;154:90–102)

Abbreviations: BrdU = 5-bromo-2′-deoxyuridine; cDNA = complementary DNA; CGRP = calcitonin gene-related peptide; DG = dentate gyrus; GFAP = glial fibrillary acidic protein; GH = growth hormone; IGF-I = insulin-like growth factor-I; IgG = immunoglobulin G; mRNA = messenger RNA; OCT = optimal cutting temperature; PBN = parabrachial nucleus; PBS = phosphate buffered saline; PCR = polymerase chain reaction; VEGF = vascular endothelial growth factor; VR-1 = vanilloid receptor-1; WT = wild type

From the Department of Translational Medical Science Research, Nagoya City University Graduate School of Medical Sciences, Nagoya; Department of Physiological Chemistry and Metabolism, University of Tokyo Graduate School of Medicine, Tokyo; Division of Reproductive Engineering, Center for Animal Resources and Development, Kumamoto University, Kumamoto, Japan.

Submitted for publication December 25, 2008, revision submitted April 19, 2009; accepted for publication May 3, 2009.

Reprint requests: Kenji Okajima, MD, Department of Translational Medical Science Research, Nagoya City University Graduate School of Medical Sciences, Kawasumi 1, Mizuho-cho, Mizuho-ku, Nagoya 467-8601, Japan; e-mail: whynot@med.nagoya-cu.ac.jp.

1931-5244/$ – see front matter

doi:10.1016/j.trsl.2009.05.001

AT A GLANCE COMMENTARY

Background

Insulin-like growth factor-I (IGF-I) exerts beneficial effects on the cognitive function by increasing synaptic transmission and inducing neurogenesis in the hippocampus. We previously reported that sensory neuron stimulation increases the IGF-I production in the mouse brain. Thus, we examined whether the stimulation of sensory neurons by capsaicin increases the hippocampal production of IGF-I, which thereby improves the cognitive function in mice.

Translational significance

The pharmacologic stimulation of sensory neurons might ameliorate cognitive functions. Our preliminary study demonstrates that donepezil, which is one of therapeutic agents for Alzheimer's disease, stimulates sensory neurons to induce IGF-I production in the mouse hippocampus.

Insulin-like growth factor-I (IGF-I) is a basic peptide composed of 70 amino acids with a ubiquitous distribution in various tissues and cells, which mediates the growth-promoting actions of growth hormone (GH) and plays an important role in postnatal and adolescent growth.[1] IGF-I has been shown to improve spatial learning by enhancing excitatory synaptic transmission in the CA_1 region of the hippocampus[2] and by inducing neurogenesis in the hippocampus.[3,4] The impaired spatial learning in mice with low serum levels of IGF-I is reversed by exogenous administration of IGF-I.[5] Furthermore, a close relation was shown between the plasma IGF-I levels and the cognitive function in older individuals.[6] These observations strongly suggest that IGF-I might improve the cognitive function by increasing the plasticity and neurogenesis in the hippocampus.

An angiogenic factor called vascular endothelial growth factor (VEGF) plays an important role in coupling angiogenesis with neurogenesis in the brain.[7] IGF-I promotes angiogenesis via a VEGF-dependent mechanism in the brain.[8] Because vascular elements are thought to be an essential feature of the stem-cell niche in the hippocampus,[9] it is possible that IGF-I promotes hippocampal neurogenesis by promoting angiogenesis.

Capsaicin-sensitive sensory neurons are nociceptive neurons that can be found in many tissues within the lining epithelia, around blood vessels, and associated with nonvascular smooth muscle and myocardium of the atria.[10] These sensory neurons release calcitonin gene-related peptide (CGRP) after activation by a wide variety of noxious physical and chemical stimuli of the vanilloid receptor-1 (VR-1) expressed on them,[11] which thereby exerts sensory-efferent functions. CGRP, which is a 37-amino acid neuropeptide, is produced by the alternative splicing of the calcitonin gene.[12] It is widely distributed in the central and peripheral nervous systems[13] and has been considered to possess diverse functions.[14] We previously reported that CGRP rapidly increases IGF-I production via increasing in its transcription in various tissues, including the brain in mice administered capsaicin.[15]

The hippocampus has been shown to receive sensory input from the parabrachial nuclei where the spinothalamic tracts terminate.[16] Nonprincipal neurons in the mouse hippocampus have been shown to be immunoreactive for CGRP.[17] CGRP receptors are expressed in astrocytes, and CGRP increases the intracellular cAMP levels in these cells.[18] Because IGF-I is synthesized in the astrocytes in the hippocampus[19] and cAMP plays an important role in the CGRP-induced increase in IGF-I production,[20] it is possible that stimulation of sensory neurons increases the IGF-I production in the astrocytes via increasing the CGRP level in the mouse hippocampus.

Based on these observations, we hypothesized that the peripheral sensory nerve stimulation by capsaicin might increase IGF-I production in the hippocampal astrocytes by increasing the CGRP levels in the hippocampus, and thereby it may increase the synaptic transmission and promote angiogenesis and neurogenesis to produce improvement of the cognitive function in mice. We examined this possibility by administration of capsaicin to wild-type (WT) mice and CGRP knockout (CGRP–/–) mice.

METHODS

Generation of αCGRP-deficient mice. The generation of αCGRP-deficient (CGRP–/–) mice was described previously.[21] The mouse CT/αCGRP genomic DNA was cloned from a BALB/c mouse genomic library in EMBL3 using synthetic oligonucleotide probes derived from the mouse CT/αCGRP complementary DNA (cDNA) sequence. A 7.0-kb fragment containing exons 3 to 5 of the mouse CT/αCGRP gene was subcloned into pBluescript (Stratagene, La Jolla, Calif). A targeting vector was constructed by replacing the 1.6-kb XbaI-XbaI fragment encompassing exon 5, which is specific for αCGRP, with the neomycin resistance gene and flanking the thymidine kinase gene. This plasmid was linearized with NotI and introduced into 129/Sv-derived SM-1 ES cells by electroporation, after which the cells were selected in a medium that contained G418 (300 μg/mL) and ganciclovir (2 μmol/L). Homologous recombinants were identified by polymerase chain

reaction (PCR) and Southern blot analysis. Targeted ES cell clones were injected into C57BL/6 mouse blastocysts to generate chimeric mice. Male chimeras were then crossbred with C57BL/6 females, and germline transmission was achieved. Littermates obtained by breeding heterozygotes with the genetic background of the 129/SvXC57BL/6 hybrid were used for phenotypic analysis. Only males were used in this study.

Genotype determination of CGRP–/– pups. Genomic DNA was extracted from tails of mice as previously described[21] and was used for PCR analysis. PCR was performed using the external primers of the replaced gene fragment. The WT allele and the mutant allele gave different band sizes. Primer sequences and PCR conditions have been described.[21]

Reagents. Human recombinant IGF-I was kindly supplied by Astellas Pharma Inc. (Tokyo, Japan). Capsaicin and 5-bromo-2'-deoxyuridine (BrdU) were purchased from Sigma Chemical Co. (St. Louis, Mo). CGRP (8-37), which is a CGRP receptor antagonist, was purchased from Peptide Institute Inc. (Osaka, Japan). An anti–IGF-I antibody was purchased from Santa Cruz Biochemistry Inc. (Santa Cruz, Calif). All other reagents were of analytical grade.

Administration of capsaicin and IGF-I. Capsaicin was dissolved in 10% Tween 20/10% ethanol (10%) with normal saline and was administered subcutaneously at dosage of 1 mg/kg as described previously.[22] Human recombinant IGF-I was dissolved in sterile distilled water and injected subcutaneously at a dosage of 0.5 mg/kg as described previously.[23]

Administration of CGRP (8-37) and anti–IGF-I antibody. CGRP (8-37) (0.1 mg/kg) was injected intravenously at 30 min before administration of capsaicin as described previously.[24] Anti–IGF-I antibody (50 μg/kg) was injected subcutaneously at 30 min before administration of capsaicin as described previously.[25,26]

Animals. Age-matched (10- to 12-week-old, 21- to 24-g) male C57BL/6 WT (Nihon SLC, Hamamatsu, Japan) and CGRP–/– mice were used in each experiment. They were maintained under standard conditions of temperature (23–25°C) and on a 12-h light/dark cycle. Food and water were provided *ad libitum*. The care and handling of the animals were in accordance with the National Institutes of Health guidelines. All the experimental procedures described below were approved by the Nagoya City University Animal Care and Use Committee. The animals were sacrificed at the end of each treatment period. The mice were anesthetized with intraperitoneally injection of ketamine (100 mg/kg) and xylazine (10 mg/kg).

Determination of hippocampus tissue levels of CGRP. The tissue levels of CGRP were determined in animals by modification of the methods as described previously.[27] The tissues were weighed and then homogenized in a polytron-type homogenizer (2× for 15 s) using 1 mL of 2 N acetic acid. The homogenates were bathed in 90°C water for 20 min and then centrifuged at 4500 g for 10 min (4°C). CGRP was extracted from the supernatant by using reverse-phase C18 columns (Amersham, Little Chalfont, UK). The columns were prepared by washing with 5 mL of methanol, followed by 10 mL of water before use. The samples were applied onto the column, followed by washing with 20 mL of 0.1% trifluoroacetic acid. CGRP was eluted with 3 mL of 60% acetonitrile in 0.1% trifluoroacetic acid, and the solvent was evaporated under a stream of nitrogen gas. The concentration of CGRP was assayed by using a specific enzyme immunoassay kit (SPI-BIO, Massey Cedex, France). The antiserum cross-reacts 100% with rodent α- and β-CGRP according to the manufactures data sheet. The results are expressed as micrograms of CGRP per gram of tissue.

Determination of hippocampus IGF-I level. The tissue levels of IGF-I were determined in animals by modification of the methods as described previously.[28] The hippocampus was minced and homogenized in a polytron-type homogenizer (2× for 15 s) using 1 mL of 1 N acetic acid according to the manufacturer's instructions. The homogenates was then centrifuged at 4500 g for 10 min. The supernatants were kept in a deep freezer at –80°C. The concentration of IGF-I was assayed by using a specific enzyme immunoassay kit (Diagnostic Systems Laboratories Inc., Webster, Tex).

Quantitative messenger RNA (mRNA) analysis. Quantitative mRNA analysis was performed as previously described.[29] The tissue was weighed and immersed in liquid nitrogen. The total RNA was extracted from the hippocampus with TRIZOL Reagent (Invitrogen, Carlsbad, Calif) according to the manufacturer's instructions. RNA extracted was used as a template for cDNA reverse transcription. Sample cDNAs were amplified in the Model 7700 Sequence detector (Perkin Elmer Japan, Chiba, Japan) with primers, dual-labeled fluogenic probes, and a Taqman PCR Reagent Kit (Applied Biosystems, Branchburgh, NJ). Thermal cycler conditions occurred for 10 min at 95°C for deactivation, as well as 40 cycles for 15 s at 95°C for denaturation and 1 min at 60°C for bath annealing and extension. The known concentrations of serially diluted IGF-I and β-actin cDNA generated by PCR were used as standards for quantitation of sample cDNA. The copy numbers of cDNA for IGF-I were standardized those for β-actin from the same sample.

Immunohistochemical staining of IGF-I and glial fibrillary acidic protein in hippocampi. The double labeling of the immunofluorescent technique was used for immunohistochemical staining of hippocampi with the anti–IGF-I antibody.[30] Mice were perfused with 4% paraformaldehyde in phosphate-buffered saline (PBS; pH 7.4). Tissue

blocks were immersed in the same perfusate at 4°C overnight and stored thereafter in a 20% sucrose solution. The tissue blocks of mouse brain were frozen in a dry-ice-cooled optimal cutting temperature (OCT) compound (Tissue Tec; Miles, Elkhart, Ind). The frozen coronal sections (18 μm thick) obtained by use of the freezing microtome were stored at –80°C before immunofluorescence. The sections were rinsed in PBS and then incubated for 1 h with PBS, 0.2% Triton X-100, and 0.5% blocking reagent (Roche Diagnostics, Basel, Switzerland) at room temperature. They were incubated overnight at 4°C with a mouse anti–IGF-I monoclonal antibody (1:200; Upstate Biotechnology, Lake Placid, NY) and rabbit antiglial fibrillary acidic protein (GFAP) polyclonal antibody (1:1000; Dako, Glostrup, Denmark). The sections were treated with secondary antibodies Alexa Fluor 568 antirabbit immunoglobulin G (IgG) for GFAP, Alexa Fluor 488 antimouse IgG for IGF-I (1:500; Invitrogen) for 1 h at room temperature. After staining, the samples were examined in a fluorescence microscope (Axio Imager A1; Carl Zeiss SMT AG, Oberkochen, Germany). The number of both IGF-I and GFAP positive cells was counted in the granule cell layer and in the hilus. The number of cells was counted using one 18-μm-thick section per animal.

***c-fos* immunohistochemistry.** Immunohistochemical staining of *c-fos* in mice brain was performed according to the method as previously described.[31] The mice were anesthetized (5% isoflurane) and decapitated. The brains were rapidly removed and frozen in dry-ice-cooled OCT compound (Tissue Tec). The frozen coronal sections (18 μm thick) obtained by use of the freezing microtome were stored at –80°C before immunofluorescence. The slides were removed from the freezer, allowed to air-dry for 15 min, and fixed for 10 min in ice-cold 4% paraformaldehyde in PBS (pH 7.4). The sections were rinsed in PBS and then incubated for 1 h with PBS, 0.2% Triton X-100, and 0.5% blocking reagent (Roche Diagnostics) at room temperature. They were incubated overnight at 4°C with rabbit anti–*c-fos* polyclonal antibody (1:500; Santa Cruz Biotechnology Inc.). The sections were treated with secondary antibodies Alexa Fluor 568 antirabbit IgG (1:500; Invitrogen) for 1 h at room temperature. After staining, the samples were examined in a fluorescence microscope (Axio Imager A1, Carl Zeiss). The number of *c-fos*–positive cells was counted in the dorsal horn (lamina I-II) of spinal cord, prabrachial nuclei, and granule cell layer, as well as in the hilus of the hippocampus. The number of cells was counted using one 18 μm-thick section per animals.

Double stain immunohistochemistry for CD31, GFAP, or calbindin-D28K with BrdU. We used BrdU labeling to monitor the proliferation and double immunofluorescent labeling for BrdU and cell-specific markers to determine

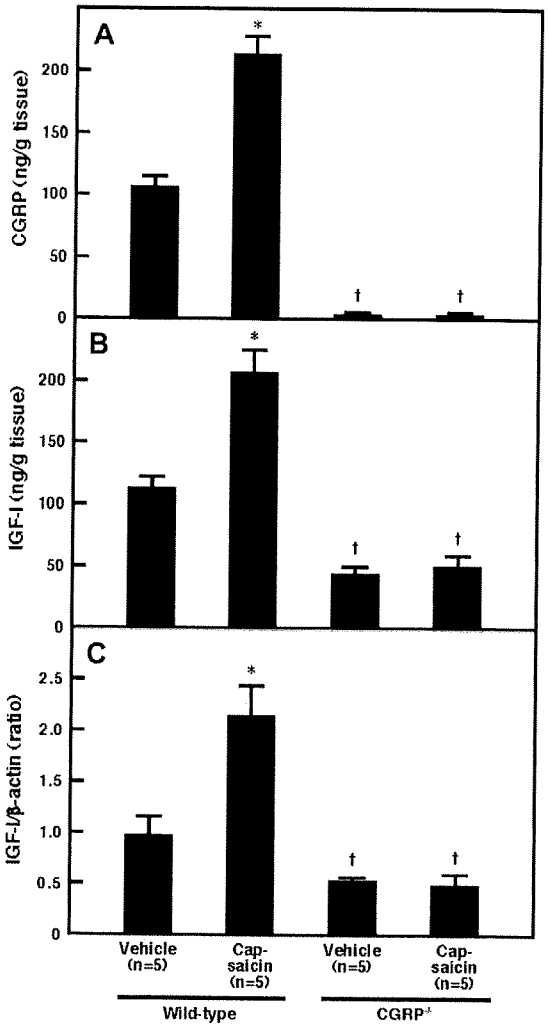

Fig 1. Effect of capsaicin administration on tissue levels of CGRP (**A**), IGF-I (**B**), and IGF-I mRNA (**C**) in the hippocampi of WT and CGRP–/– mice. The tissue was removed 30 min after subcutaneous injection of capsaicin (1 mg/kg) or vehicle. The values are expressed the means ± standard deviation (SD) derived from 5 animal experiments. $^{*}P < 0.01$ vs vehicle; $^{\dagger}P < 0.01$ vs WT.

the phenotype of the progenitor progeny. BrdU was dissolved in sterile saline and injected intraperitoneally at a dosage of 50 mg/kg 30 min before administration of capsaicin as described previously.[4] Angiogenesis and neurogenesis in the mouse brains was monitored by BrdU incorporation into the nuclei of dividing cells as previously described.[4] The samples were treated for DNA denaturation in the following manner: The tissues were incubated in 50% formamide in 2 × SSC buffer (1 × SSC, 0.3 mol/L NaCl, and 0.03 mo/L sodium citrate) at 65°C for 2 h, rinsed in PBS and then incubated for 30 min with 2 N HCl at 37°C. They were rinsed for 10 min at room

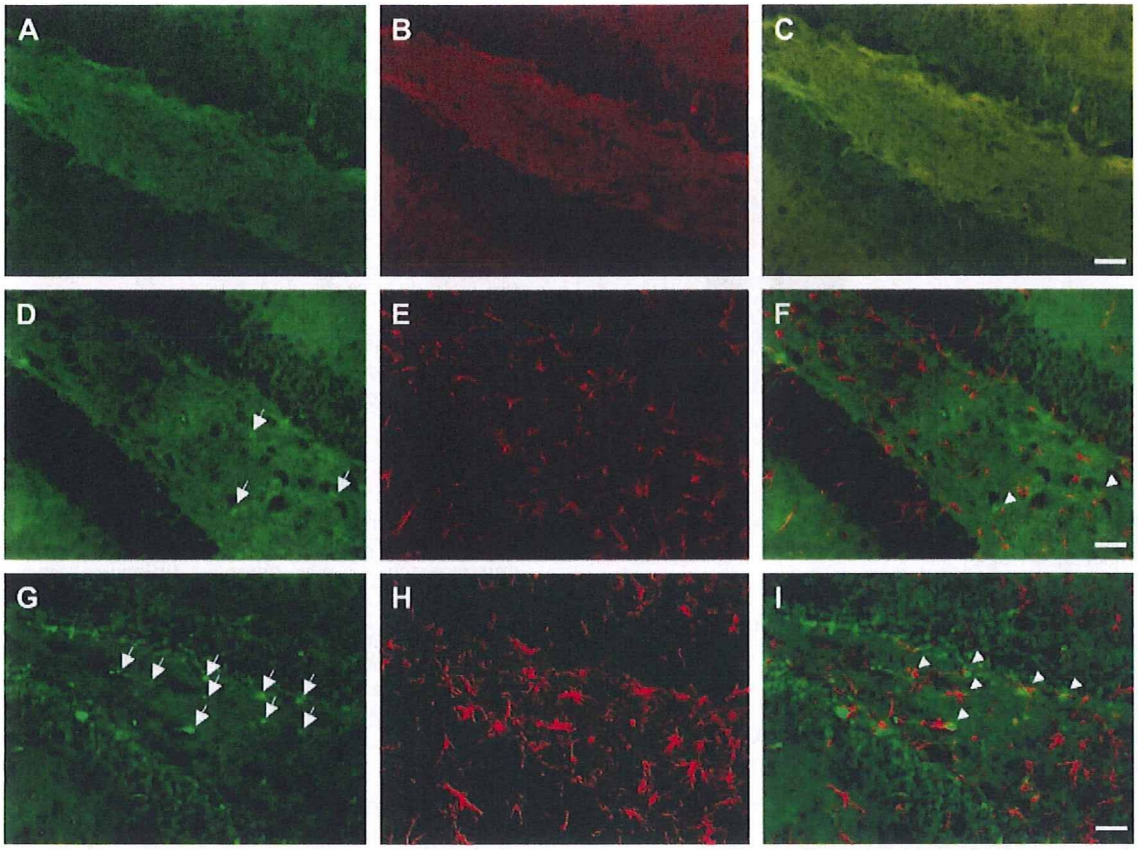

Fig 2. Effect of capsaicin administration on immunohistochemical expression of IGF-I in the hippocampi of WT mice. Fluorescent photomicrographs of cryostat sections showing the expression of IGF-I in the hippocampi of WT mice were shown. Double labeling of IGF-I (green) and GFAP (red) showed the localization of IGF-I in the hippocampi. Vehicle (**D–F**) or capsaicin (1 mg/kg) (**G–I**) was injected subcutaneously, and tissues were removed 30 min after capsaicin injection. The arrows indicate IGF-I positive staining. The arrowheads indicate colocalization of IGF-I and GFAP positive staining. The fluorescent photomicrographs in **A–C** were negative controls in which neither anti–IGF-I nor anti-GFAP antibodies were used. Five animals in each group were examined, and the typical results are shown. Scale bars = 25 μm in **C**, **F**, and **I**.

temperature in 0.1 mol/L boric acid (pH 8.4). The tissue was rinsed in PBS 3 times, followed by incubation in PBS, 0.2% Triton X-100, and 0.5% blocking reagent (Roche Diagnostics) for 1 h and then with primary rat anti-CD31 monoclonal antibody (1:200; BD Biosciences PharMingen, San Diego, Calif) with mouse anti-BrdU monoclonal antibody (1:100; Invitrogen), rabbit anti-GFAP polyclonal antibody (1:1000; Dako), or mouse anti-calbindin-D28 K monoclonal antibody (1:200; Abcam, Cambridge, UK) with rat anti-BrdU monoclonal antibody (1:400; Abcam) overnight at 4°C. The sections were treated with secondary antibodies Alexa Fluor 594 antirat IgG for CD31, Alexa Fluor 488 antimouse IgG for BrdU (antimouse), Alexa Fluor 568 antirabbit IgG for GFAP, Alexa Fluor 488 antimouse IgG for calbindin-D28 K, and Alexa Fluor 594 antirat IgG for BrdU (antirat) (1:500; Invitrogen) for 1 h at room temperature. After staining, the samples were examined in a fluorescence microscope (Axio Imager A1; Carl Zeiss). BrdU-positive cells were counted in the granule cell layer and in the hilus. The number of cells was counted using one 18-μm-thick section per animals.

Morris water maze task. Behavioral testing was conducted as described previously.[32,33] We used a circular pool (150 cm diameter) filled with water at 30°C, which contained a round-shaped transparent acrylic platform (12 cm diameter). In the task, the platform was submerged 1 cm below the surface of the water and located in the southeast quadrant of the pool throughout the trials. After the mouse was put into the pool, each had a maximum of 90 s to locate and climb onto the platform (1 trial). When a mouse located the platform, it was

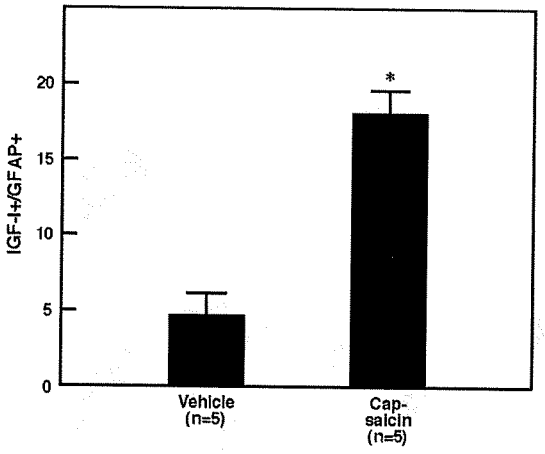

Fig 3. Effect of capsaicin on the number of cells showing colocalization of IGF-I- and GFAP-positive staining in the hippocampus of WT mice. Values are means ± SD derived from 5 animal experiments. *$P < 0.01$ vs vehicle.

allowed to stay on it for 20 s. Mice that did not find the platform in the allowed time were placed on it by the experimenter and left there for 20 s. The latency to reach the platform was monitored. Each mouse was subjected to 1 trial per day. The task consisted of 8 days of trials.

Statistical analysis. Data are expressed as the mean ± SD. The results were compared using an analysis of variance followed by Scheffé's post hoc test. A P level of $\leq .05$ was considered statistically significant.

RESULTS

Effect of capsaicin administration on the tissue levels of CGRP, IGF-I, and IGF-I mRNA in the hippocampi of WT and CGRP–/– mice. To examine whether capsaicin increases both the tissue levels of IGF-I and the expression of IGF-I in the mouse hippocampus through sensory neuron stimulation, we determined the tissue levels of CGRP, IGF-I, and IGF-I mRNA in the hippocampi of WT and CGRP–/– mice at 30 min after the subcutaneous administration of capsaicin. The baseline tissue levels of CGRP, IGF-I, and IGF-I mRNA in the hippocampus of WT mice were significantly higher than those in that of CGRP–/– mice ($P < 0.01$) (Fig 1, *A–C*). Furthermore, administration of capsaicin significantly increased the hippocampal tissue levels of CGRP, IGF-I, and IGF-I mRNA in WT mice ($P < 0.01$), whereas no such increase of these levels was noted in the hippocampus of CGRP–/– mice (Fig 1, *A–C*).

Effect of capsaicin administration on the immunohistochemical expression of IGF-I in the hippocampus of WT mice. An increase in the immunohistochemical expression of IGF-I in the dentate gyrus (DG) was observed at 30 min after capsaicin administration (Fig 2, *D* and *G*). The IGF-I immunoreactivity was colocalized with the immunoreactivity for the astrocyte marker GFAP in WT mice (Fig 2, *D–F*), and an increase of the IGF-I immunoreactivity colocalized with GFAP immunoreactivity was observed following capsaicin administration in WT mice (Fig 2 *G–I*, and Fig 3).

Effect of capsaicin administration on the *c-fos* expression in the spinal and supraspinal nervous tissues in WT and CGRP–/– mice. To analyze the mechanism and pathway of the capsaicin-induced relay system that might lead to the increase in the hippocampal IGF-I production in WT mice, we analyzed the *c-fos* expression levels in the spinal and supraspinal nervous tissues in WT and CGRP–/– mice after administration of capsaicin. In WT mice, an increase of *c-fos* expression was observed at 120 min after capsaicin administration was increased in the dorsal horn (lamina I-II) of the spinal cord and, supraspinally, in the parabrachial nuclei (PBN) and DG (Figs 4–6).[34-37] In contrast, no increase of *c-fos* expression was observed after capsaicin administration in these tissues in CGRP–/– mice (Figs 5 and 6).

Effect of capsaicin administration on the hippocampal angiogenesis and neurogenesis in WT and CGRP–/– mice. The colocalization of BrdU immunoreactivity

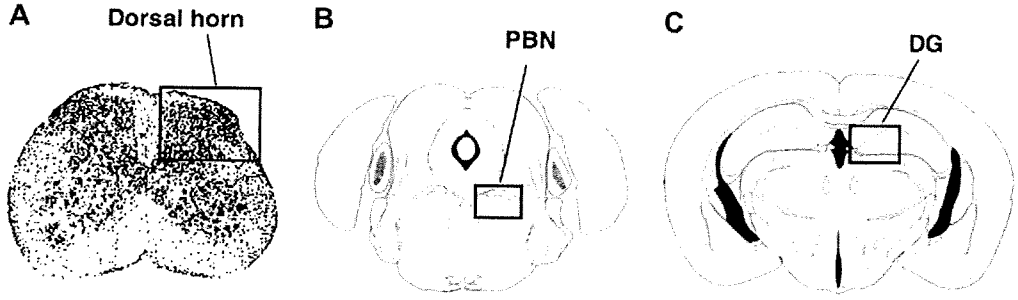

Fig 4. Schematic diagrams of spinal cord (**A**) or brain sections (**B** and **C**) adapted from the atlas of the mouse spinal cord[36] or the mouse brain atlas,[37] respectively, where select spinal cord or brain regions were analyzed for *c-fos* expression. The location and the approximate size of the analyzed area for each region is indicated. **A**, Dorsal horn of spinal cord; **B**, PBN, medial parabrachial nucleus of the pons; **C**, DG, granular cell layer of the DG.

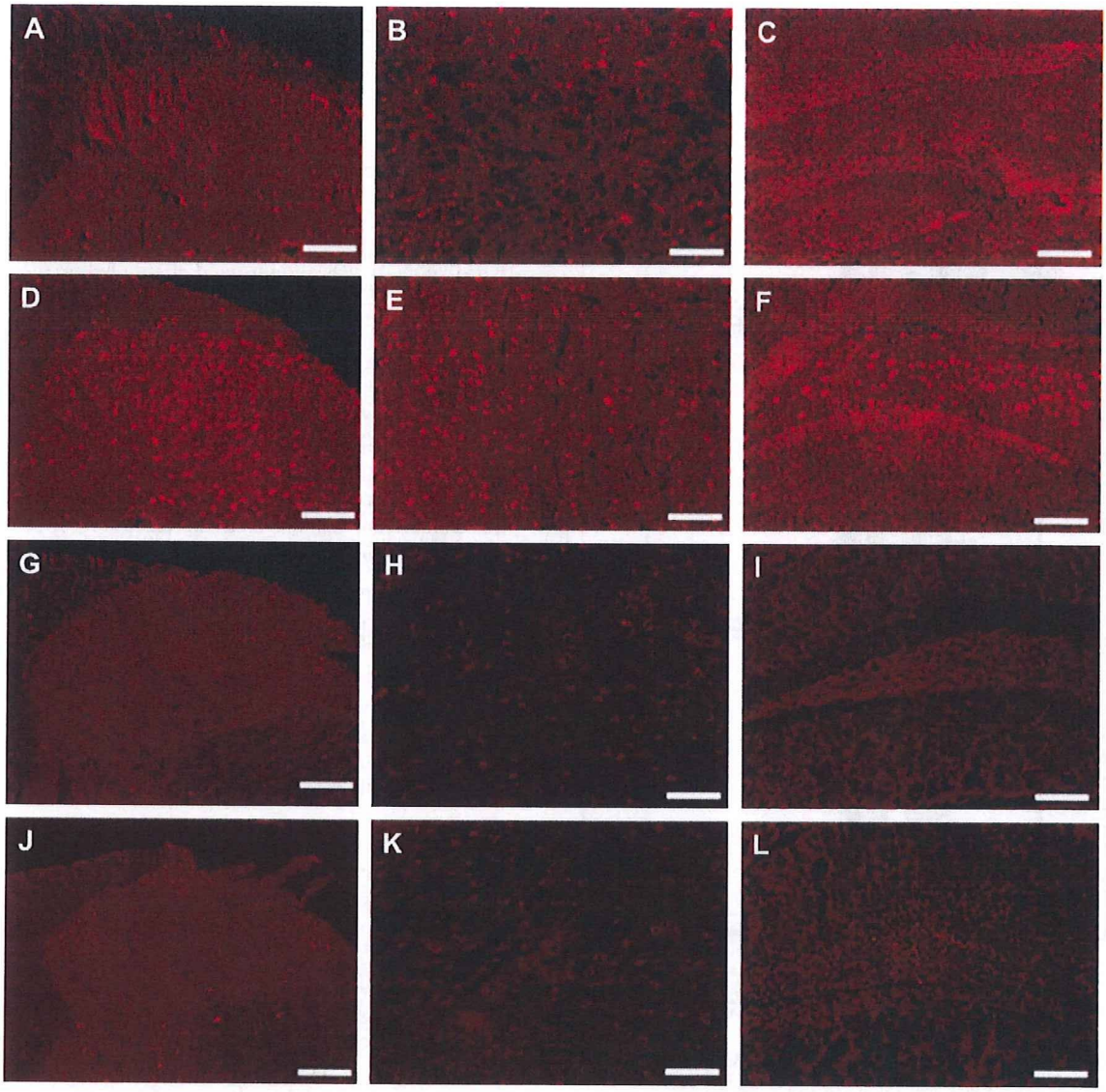

Fig 5. Effect of capsaicin administration on the *c-fos* expression in the spinal and supraspinal tissue levels in WT mice and CGRP–/– mice. All tissues were removed 120 min after subcutaneous injection of capsaicin (1 mg/kg) (**D–F** = WT mice, **J–L** = CGRP–/– mice) or vehicle (**A–C** = WT mice, **G–I** = CGRP–/– mice). The immunohistochemial expression of *c-fos* represents the dorsal horn of the spinal cord indicated in Fig 3, *A* (**A**, **D**, **G**, and **J**); the medial brachial nucleus indicated in Fig 3, *B* (**B**, **E**, **H**, and **K**); or granular cell layer of the DG indicated in Fig 3, *C* (**C**, **F**, **I**, and **L**). Five animals in each group were examined, and the typical results are shown. Scale bars = 100 μm.

with immunoreactivity for the vascular endothelial cell marker CD31, the granule cell marker calbindin-D28 K, and the astrocyte marker GFAP were examined to determine the phenotype of the progenitor cell progeny in the DG after capsaicin administration in WT and CGRP–/– mice (Figs 7 and 8). The immunohistochemical expression of CD31, calbindin-D28 K, and BrdU in the hippocampus of WT mice at 30 min after capsaicin administration was shown in Fig 7. The number of BrdU-immunoreactive cells in the DG was significantly higher in WT mice than in CGRP–/– mice ($P < 0.01$) (Fig 8, *A*). Furthermore, a significant increase in the number of BrdU-immunoreactive cells was observed in the DG at 30 min after capsaicin administration in WT mice ($P < 0.01$) (Figs 7 and 8), whereas no such increase was observed in CGRP–/– mice (Fig 8, *A*).